NUMERICAL SIMULATION FOR FINDING THE EFFECT OF BLOCKAGE AND TUNNEL INTERFERENCE IN WIND TUNNEL TESTING OF A BLUFF BODY

Thesis Submitted in Partial Fulfillment of the Requirements for the Degree of

Master of Engineering in Mechanical Engineering

By

SARANGRAB ROY CHOWDHURY

[Examination Roll No: M4MEC24001]

[University Registration No: 163702 of 2022-2023]

Under the Guidance of

Dr. PRANIBESH MANDAL

DEPARTMENT OF MECHANICAL ENGINEERING

FACULTY OF ENGINEERING & TECHNOLOGY

JADAVPUR UNIVERSITY

KOLKATA – 700032

MAY 2024

FACULTY OF ENGINEERING AND TECHNOLOGY

JADAVPUR UNIVERSITY

CERTIFICATE OF APPROVAL*

This foregoing thesis is hereby approved as a credible study of an engineering subject carried out and presented in a manner satisfactory to warrant its acceptance as a prerequisite to the degree for which it has been submitted. It is understood that by this approval the undersigned do not endorse or approve any statement made, opinion expressed or conclusion drawn therein but approve the thesis only for the purpose for which it has been submitted.

COMMITTEE ----------

ON FINAL EXAMINATION FOR

EVALUATION OF THE THESIS ----------

***Only in case the thesis is approved**

FACULTY OF ENGINEERING AND TECHNOLOGY

JADAVPUR UNIVERSITY

CERTIFICATE OF RECOMMENDATION

I hereby recommend that the thesis presented under my supervision by ***SRI SARANGRAB ROY CHOWDHURY*** *entitled* "**Numerical Simulation for Finding the Effect of Blockage and Tunnel Interference in Wind Tunnel Testing of a Bluff Body**" *be accepted in partial fulfillment of the requirements for the degree of* ***Master of Engineering in Mechanical Engineering****.*

Countersigned

Thesis Supervisor

Head of the Department
Department of Mechanical Engineering

Dean
Faculty of Engineering and Technology

DECLARATION OF ORIGINALITY AND COMPLIANCE OF ACADEMIC ETHICS

I hereby declare that the thesis contains literature survey and original research work by the undersigned candidate, as a part of his ***MASTER OF ENGINEERING IN MECHANICAL ENGINEERING*** studies. All information in this document have been obtained and presented in accordance with the academic rules and ethical conduct.

I also declare that, as required by these rules of conduct, I have fully cited and referenced all the material and results that are not original to this work.

Name: **SARANGRAB ROY CHOWDHURY**

Examination Roll Number: **M4MEC24001**

Class Roll Number: **002211202003**

University Registration No: **163702 of 2022-2023**

Thesis Title: ***Numerical Simulation for Finding the Effect of Blockage and Tunnel Interference in Wind Tunnel Testing of a Bluff Body***

Signature with Date:

ACKNOWLEDGEMENT

.

I acknowledge my deepest gratitude to my thesis supervisor, Dr. Pranibesh Mandal, Assistant Professor, Department of Mechanical Engineering, Jadavpur University for his invaluable guidance, support and encouragement throughout the research process. His expertise and unwavering commitment have been instrumental in shaping this thesis. I am grateful for this opportunity and look forward to continue my interaction with him in the future.

I extend my appreciation to all the staff and laboratory assistants of the Hydraulics Laboratory, Department of Mechanical Engineering, Jadavpur University who have provided me with excellent working conditions.

I am also thankful to all of my batchmates who have created a lively atmosphere within the laboratory. The support and cooperation from several research scholars are also worth mentioning.

Last, but mot the least, I would like to heartily thank my parents, whose constant support has made writing this thesis possible.

Date: May 2024

(SARANGRAB ROY CHOWDHURY)

CONTENTS

Chapter **Page**

LIST OF TABLES

Table **Page**

LIST OF FIGURES

Figure **Page**

NOMENCLATURE

Symbol	Significance
ρ	Density of air
g	Acceleration due to gravity
ζ	Shear stress
$\boldsymbol{u}$	Velocity vector
P	Pressure
Re	Flow Reynolds' number
C_D	Coefficient of drag
$C_{D,error}$	Difference in drag coefficient between confined and unconfined flow
$C_{D,error,supp.sys.}$	Difference in drag coefficient between mounted and unmounted conical body
β	Blockage ratio

ABSTRACT

Flows past bluff bodies are ubiquitous in various engineering applications, such as flows past tall buildings, bridge piers, undersea pipelines, and launch vehicles. These flows exhibit complex phenomena, prompting extensive experimental and numerical investigations to unravel their intricacies. Wind tunnel testing is a pivotal experimental technique employed to analyse flow patterns around objects, notably used to determine drag coefficients for aircraft. However, the accuracy of wind tunnel tests is often compromised by blockage effects, where the rigid tunnel walls impede the free lateral displacement of the fluid stream around the body, leading to "tunnel interference". This interference causes the streamlines to converge near the body, resulting in higher velocities than those in an unbounded stream.

This study addresses the necessity to quantify the impact of blockage ratio on flow characteristics around a bluff body. The blockage ratio, defined as the ratio of the model's projected area to the wind tunnel's cross-sectional area, significantly influences experimental outcomes. Additionally, supporting systems used to mount models in wind tunnels introduce "supporting system interference", where the interaction between the system and the body's wake alters drag measurements. These systems affect the wake width and velocity gradients near the body, thereby increasing skin friction drag and total drag. A comprehensive review of the literature on blockage effects and supporting system interference has been conducted. The study provides a detailed examination of how blockage ratio and supporting systems impact drag measurements.

In this investigation, numerical simulations have been performed to study the axial flow of air past conical bluff bodies in both confined and unconfined flow domains. The drag coefficient has been computed numerically for each scenario, and the difference in drag coefficients between confined and unconfined flows has been plotted against the Reynolds number, illustrating the tunnel interference effect. Furthermore, to assess support interference, each conical bluff body has been mounted on a supporting system within a confined domain, and the resulting drag coefficient has been compared to that of an unsupported body. The variations in drag coefficient due to the supporting system have also been plotted against the Reynolds number.

The findings reveal significant insights into the effects of tunnel interference and support interference on drag measurements. Quantifying these effects is crucial for improving the accuracy of wind tunnel tests, thereby enhancing the reliability of experimental data used in designing and optimizing engineering structures subjected to bluff body flows. This study underscores the importance of considering both blockage and support effects in experimental setups and provides a foundation for future research to mitigate these interferences in wind tunnel testing.

Chapter 1:

Introduction and Literature Review

1.1. Interference of wind tunnel walls

Flows past bluff bodies are ubiquitous in many engineering applications, including flows past tall buildings, bridge piers, undersea pipelines, launch vehicles, etc. Hence numerous experimental and numerical studies have been conducted to understand the complex phenomena that emerges with these kinds of flows. One of these experimental studies is the wind tunnel testing. Wind tunnel tests are primarily performed to analyse the flow patterns around a vehicle or object. A major application of wind tunnel testing is to determine the drag coefficients generated around an aircraft during flight. However, blockage effects tend to make the results of these tests inaccurate. The rigid boundaries of the tunnel walls prevent a free lateral displacement of the fluid stream caused by the body. This causes the streamlines of the flow to converge in the neighbourhood of the body and the velocities become greater than what they would have been in an unlimited stream. This is what is called the "tunnel interference" and experiments conducted in wind tunnels are susceptible to such effects. Hence it was imperative to quantify the effect of blockage ratio on the flow characteristics around a bluff body. A huge volume of literature discussing this problem exists, a review of which has been provided herein. Before reviewing the literature, however, the expressions of both the coefficient of drag and blockage ratio has been given.

The coefficient of drag, C_D is given as the ratio of drag force on the body to the product of dynamic pressure and projected area on the body.

The blockage ratio, by definition, is given by the ratio of the projected area of the model to the area of cross-section of the wind tunnel.

The blockage effect on bluff bodies has been extensively discussed by Maskell (1963) **[1]** where he deduces an empirical expression for the effective increase in dynamic pressure of the flow due to the blockage effect, as a function of the blockage ratio. Blockage ratio is defined as the ratio of the projected area of the bluff body to the cross-section area of the tunnel or channel. V.J. Modi and S.E. El-Sherbiny (1977) **[2]** presented a potential flow model for 2-dimensional symmetric bluff bodies under wall confinement, which provided a procedure for predicting surface pressure loading on a bluff body over a range of blockage ratios. This theoretically predicted that the presence of boundary layers on tunnel walls indeed affect pressure distribution over a body, a phenomenon termed as "tunnel interference". This theoretical prediction was later confirmed experimentally by Petty (1979) **[3]** who observed that when the blockage ratio was 0.5, there was a 10 % change in maximum pressure on the surface of the body.

The effect of blockage ratio on confined flow has been documented by R.N. Mondal and M.M. Alam (2023) **[4]** where they state that when the blockage ratio is sufficiently small, there is not a significant deviation of the results for confined flow from the actual free stream flow. However, when the blockage ratio becomes large enough such that the boundary layers of the tunnel wall interact and modifies the flow around the body, the deviation is significant. They also stated that a square cylinder undergoes a greater blockage effect than a circular cylinder.

The most common shapes that are used for investigation of blockage ratio effects on bluff bodies are circular cylinders, square cylinders and flat plates. Stanlaker and Hussey (1979) **[5]** studied the wall effect due to transverse motion of a long length small diameter cylinder in a Newtonian fluid. The effect of the wall on the dimensionless drag coefficient was grouped into strong boundary and weak boundary regions. The effect was seen to be less in weak boundary zone than in the strong boundary zone. Chakraborty et al. (2004) **[6]** reported that for a fixed

Reynolds' number (Re), the drag coefficient decreases with an increase in blockage ratio for the range blockage ratio = 0.05-0.65. However, the simulations conducted by Kumar and Singh (2020) **[7]** indicate that for a confined flow past a circular cylinder, the mean drag coefficient decreases with Re for a fixed blockage ratio and increases with blockage ratio for a fixed Re for the range of Re = 5000-15000). For low blockages, such problems have also been studied numerically by Kannaris et.al. (2011) **[8]** , Ooi et. al. (2020) **[9]** and Nguyen and Lei (2021) **[10]**. It has been found that at low blockage ratios, vortex shedding is present but the standard Karman wake has been inverted causing shed vortices to cross the centre plane.

Compared to the study of confined circular cylinder, the study of confined square cylinder received less attention. Based on numerical simulations of a highly confined flow past a square cylinder, Mishra et. al. (2019) **[11]** showed that the drag coefficient is of the order of magnitude of 10^3, which is significantly higher than the 47 that was found out in the unconfined case by Sohankar et. al**.** (1999) **[12]** . The investigation carried out by Mukhopadhyay et.al. (1992) **[13]** showed that confinement stabilises the wake structure around a square cylinder and that the drag coefficient as well as the base stagnation and suction pressures increase with an increase in the blockage ratio.

There have been studies conducted on confined flow past a flat plate. A notable contribution in this topic was done by Takeuchi and Okamoto (1983) **[14]**. They experimentally showed that for blockage ratio = 0-0.4 and Re = 3.22×10^4, the mean drag coefficient increases monotonically with blockage ratio.

Considerable importance has also been given to study of confined flows past spherical bodies. Uhlherr and Chhabra (1995) **[15]** showed that the drag coefficient of a sphere falling through a channel depends on both the sphere-to-channel diameter ratio and the Reynolds' number. They arrived at the following

equation to estimate the relationship between drag coefficient and Reynolds' number for unconfined flow as

$C_D Re^2 = \text{constant}$ (3)

Similar results were also obtained by Chhabra et. al. (2003) **[16]** where it was reported that drag coefficient for a sphere falling through a cylindrical tube varied with both Reynolds' number and diameter ratio at intermediate Reynolds' numbers. Hydrodynamics study of laminar flow of a Newtonian fluid past a hot confined sphere was conducted by Krishnan and Kaman (2010) **[17]**. They found that the wall effect was more predominant at lower Reynolds' numbers, whereas the accuracy of predicting wall effects have become better at higher Reynolds' numbers.

For the case of unconfined flows past a bluff body, considerable volume of literature exists. Of the few earliest works in this field, the numerical analysis of Kuwaguti and Jain (1966) **[18]** is notable. They obtained steady-state solutions for flow past a circular cylinder in an unconfined domain up to Re = 50. Their work was refined and expanded upon by Hamielec and Raal (1969) **[19]** who formulated results up to Re =500. Dennis and Chang (1970) **[20]** were also able to obtain steady-state solution for unconfined flow past a circular cylinder, using finite difference approximation, using a stream function-vorticity formulation. The mean drag coefficient for the same problem was also formulated by Sucker and Brauer (1975) **[21]**. Fornberg (1980 and 1985) **[22a, 22b]** has also published a lot of results for this problem for the range of $20 < Re < 600$. More recently, Rajani et. al. (2009) **[23]** computed the force components up to Re = 200. Chakraborty et. al. **[6]** also tabulated a few results for this unconfined flow (which included coefficient of drag and coefficient of surface pressure) as validation of their work, which complied quite well to the aforementioned literature.

Other than conventional shapes of bluff bodies, Dhiman and Shyam (2011) **[23]** and Chatterjee and Mondal (2012) **[24]** studied the flow and heat transfer

characteristics over an equilateral triangle in the Reynolds' number range of 50-200.

Although there seems to be no dearth in literature dealing with unconfined flows, very few of them deal with air (or any compressible fluid) as the working fluid. One such paper was published by Pawar et. al. (2020) **[25]** which found the force coefficients as well as the wake structure of unconfined flow past a circular cylinder in the range of $0 < Re < 160$ and for angles of attack varying from 0^0 to 180^0. Moreover, most of the studies have considered only a few shapes for bluff bodies (square cylinder, circular cylinder and flat plate) while there is very limited information regarding confined or unconfined flow past bluff bodies of any other shapes. One of the earliest works in this field is that of List and Schemeneaur (1971) **[26]** who listed a few points on coefficient of drag versus Reynolds' number. Later, Sharma and Chhabra (1991) **[27]**, who described experimentally the effect of blockage ratio on coefficient of drag in cones free-falling in Newtonian as well as non-Newtonian fluids. The study was carried out using unconfined flow Reynolds number which varied in the range of very low to 500 as the system parameter. In their study, the cone angle was varied in the range of 43^0–93.7^0. The flow behaviour index, n was kept in the range of 1.0–0.62 with the consistency index, m of $3.73 \text{ X } 10^{-3} < m < 4$ Pa.s^n. The ratio of the cone to flow channel diameters was also varied in the range of 0.148–0.4343. The wall effect, f was found independent of the apex angle and power law index but affected by the diameter ratio and Reynolds number. They also arrived at a mathematical equation to fit their experimental data.

Their work was later expanded by Samantaray et. al**.** (2017) **[28]**, who numerically found the correlation between coefficient of drag and blockage ratio for conical, cylindrical and spherical bluff bodies.

1.2. Interference of model supporting system

In most of the experiments performed in wind tunnels, the model is mounted on some kind of supporting systems. The supporting systems, are responsible not only to hold the model in place, but also, in most cases, to measure the forces an moments that the body experiences. Due to the presence of such supporting systems, the drag force experienced by the body is altered somewhat and hence the results recorded in the become inaccurate to some extent. The reason for these inaccuracies can be attributed to the fact that the supporting system interacts with the wake behind the body and increases the wake width. Also, due to the presence of the boundary layers on the supporting system, the velocity gradients close to the body increases and thus the skin friction drag increases. As a result, the total drag on the body increases. This effect is known as the "supporting system interference".

There is very little available literature on the effect of supporting system interference on the measurement of drag. The experimental work of Ocokoljic et. al. (2017) **[29]** has shed some light on the support system interference on the aerodynamic characteristics of an aircraft model. They found out that the presence of a bent sting balance increases the drag coefficient but decreases the lift coefficient on the aircraft while both cruising as well as take-off. Cartieri et. al. (2012) **[30]** quantified the effect of support system on the "force distortion" of the body. They correlated the data from experimental investigation and CFD simulations to find out the amount of correction of inlet Mach number required to imitate the actual unconfined flow. A similar analysis was carried out by Mouton (2009) **[32]** who found little variations of drag between CFD simulations (unconfined flow) and the actual wind tunnel testing of the aircraft with support systems. The agreement at Mach 0.85 was still within 2 X 10^{-4} up to a lift coefficient of 0.4, then deteriorates to about 5 10^{-4}. At Mach 0.87, the gap between CFD and experiments is constant at about 5 X 10^{-4}.

From the aforementioned literature, it can be seen that there are two sources of error in drag measurement, (i) tunnel interference and (ii) supporting system interference. In all of the works mentioned above, the influence of either one of these have been discussed. However, while performing wind tunnel testing, the error that will arise while measuring drag will be due to a combined effect of both these interferences. This is because, in a wind tunnel test, the model will almost always be mounted on a supporting system; and clearly the wind tunnel provides a confined flow. So, in the present study, the error in drag measurement due to the cumulative effect of tunnel interference and supporting system interference on a conical body has been computed.

1.3. Statement of the problem

Numerical study of axial flow of air past conical bluff bodies is considered in this study. Coefficient of drag has been computed numerically for both confined and unconfined flow domains. The difference in drag coefficient between confined and unconfined flows has been determined and plotted against the Reynolds' number of the flow. This gives us the effect of tunnel interference on the coefficient of drag. To quantify the effect of support interference, each conical bluff body was mounted on a supporting system and drag coefficient was found for flow in confined domain. The difference in drag coefficient between supported body and unsupported body has then been evaluated and plotted against flow Reynolds' number.

Chapter 2:

System Description and Meshing

2.1. Description of the physical system

In the present study, the behaviour of axial flow of air past conical bluff bodies are numerically studied. The drag coefficients of the bodies are calculated and the effect of tunnel interference and blockage ratio on the drag coefficient is discussed. For the purpose of understanding the effect of blockage ratio on coefficient of drag, four geometrically similar conical bluff bodies were considered. The detailed geometric specifications of these bodies have been provided in table 1 below. The shape of the bodies is chosen so as to bear resemblance to atmospheric re-entry vehicles.

For simulating confined and unconfined flow, each of these cones have been put inside "finite" and "infinite" domains, the specifications of which have been mentioned below. The models of the bodies have been shown in figure 1 below.

Table 1: Geometric specifications of the cones

Cone No.	Base Diameter (d) (mm)	Length (l) (mm)
1	50	80
2	100	160
3	150	240
4	200	320

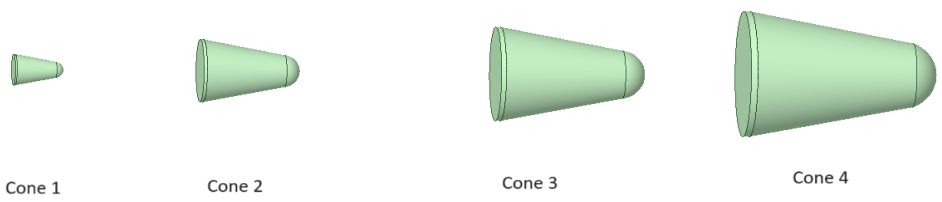

Fig 1: Models of the cones used in simulation

The geometric dimensions of the supporting system mentioned above are acquired from the dimensions of a sting balance in the laboratory. The height of the balance is taken as 224 mm and the dimensions of the base are 190 mm X 120 mm.

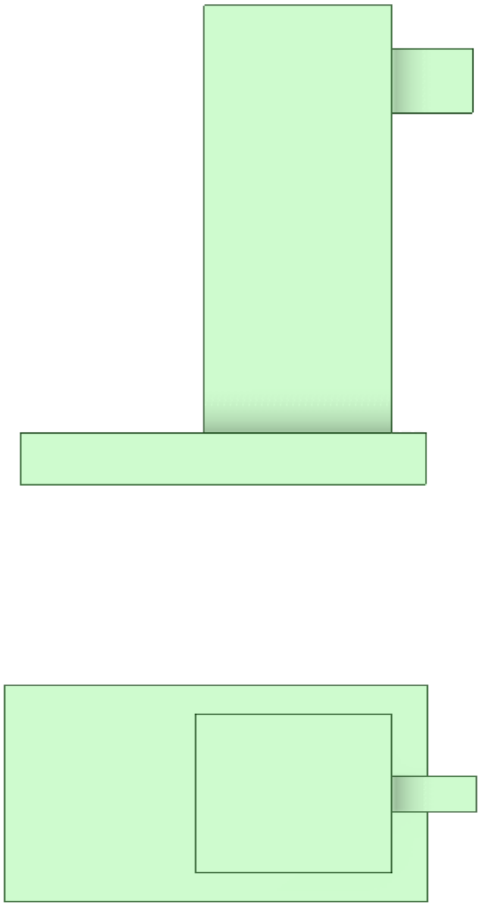

Fig 2: The supporting system used in the simulations

Since the finite domain is meant to simulate flow conditions during a wind tunnel testing, a cross-section area of 1 m X 1 m is considered for it. However, for the infinite flow domain, a cross-section area of 4 m X 4 m has been chosen, the reason for which is explained later.

The geometries of the cones and the flow domains have been created using the SpaceClaim (SC) feature of ANSYS Workbench. After creation of the models,

the meshing is important for the purposes of finding the solution. The element size and number of modes are adjusted with the geometry and size of the bodies and the blockage ratio. The display of mesh for all the bodies have been shown in figures 5, 6 and 7 below.

2.2. Mathematical modelling

Steady-state equation of continuity and momentum equations are solved together to obtain velocity and pressure fields. Based on the pressure and velocity fields, the coefficient of drag was obtained using equation 1.

$$\nabla.(\rho u) = 0$$
$$\nabla.(\rho uu) = -\nabla P + \nabla\zeta + \rho g \quad (1)$$

Since the flow to be modelled was turbulent, the Generalized K-Omega (GEKO) model was used to model the turbulent stresses.

GEKO is a two-equation model, based on the k-ω model formulation, but with the flexibility to tune the model over a wide range of flow scenarios. The key to such a strategy is the provision of free parameters which the user can adjust for specific types of applications without negative impact on the basic calibration of the model. In other words, instead of providing users flexibility through a multitude of different models, the current approach aims at providing one framework, using different coefficients to cover different application sectors.

The main characteristic of GEKO is that it has several free parameters for tuning the model to different flow scenarios. The starting point of GEKO is the equations given below.

The free coefficients of the GEKO model are implemented through the functions F_1, F_2 and F_3 which can be tuned by the user according to the flow conditions. Currently there are six parameters included for that purpose:

• C_{SEP}

- Main parameter for adjusting separation prediction for boundary layers - Affects all flows

- Increasing C_{SEP} reduces eddy-viscosity leading to more sensitivity to adverse pressure gradients for boundary layers and to lower spreading rates for free shear flows (compensated by C_{MIX})

• C_{NW}

- Affects mostly the inner part of wall boundary layers (limited to no impact on free shear flows.

- Increasing C_{NW} leads to higher wall shear stress and wall heat transfer rates in nonequilibrium flows.

- Effect on non-generic flows (e.g. vortices) moderate but not systematically tested

- Users can mostly use C_{NW} = 0.5 (default)

• C_{MIX}

- Affects only free shear flows (boundary layer shielded due to function F_{blend}). - Increasing C_{MIX} increases spreading rates of free shear flows.

- For each value of C_{SEP} an optimal value of C_{MIX} exists, which maintains optimal free shear flows. This value is given by the correlation C_{MIX}=C_{MixCor} which is default $C_{MixCor} = 0.35\text{sign}(C_{Sep} - 1)\sqrt{(|CS_{ep} - 1|)}$

• C_{JET}

- Is active in a sub-model of C_{MIX} (no impact for C_{MIX} = 0).

- Affects mostly jet flows. Increasing C_{JET} while C_{MIX} is active, decreases spreading rate for jets.

- Allows to adjust spreading rate of jet flows while maintaining spreading rate of mixing layer.

- Users can mostly use C_{JET} = 0.9 (default)

- Has no effect in case of C_{MIX} = 0

• C_{CORNER}

- Non-linear stress-strain term to account for secondary flows in corners

• C_{CURV} - An existing model for curvature correction

All coefficients (except of C_{JET} which is of minor importance) can be accessed globally or locally through User Defined Functions (UDFs), allowing a global or zonal model optimization.

The coefficients C_{SEP} and C_{NW} affect boundary layers, whereas C_{MIX} and C_{JET} are designed for free shear flows.

Any further information on the GEKO model can be obtained from Menter et. al. (2021) **[33]**.

The governing equations of the GEKO model has been given in equation 6.

$$\frac{\partial(\rho k)}{\partial t}+\frac{\partial\left(\rho U_j k\right)}{\partial x_j}=P_k-C_\mu\rho k\omega+\frac{\partial}{\partial x_j}\left[\left(\mu+\frac{\mu_t}{\sigma_k}\right)\frac{\partial k}{\partial x_j}\right]$$

$$\frac{\partial(\rho\omega)}{\partial t}+\frac{\partial\left(\rho U_j\omega\right)}{\partial x_j}=C_{\omega1}F_1\frac{\omega}{k}P_k-C_{\omega2}F_2\rho\omega^2+\rho F_3CD+\frac{\partial}{\partial x_j}\left[\left(\mu+\frac{\mu_t}{\sigma_\omega}\right)\frac{\partial\omega}{\partial x_j}\right]$$

$$\mu_t=\rho\nu_t=\rho\frac{k}{max(\omega,S/C_{Realize})}$$

$$P_k=-\tau_{ij}\frac{\partial U_i}{\partial x_j}$$

$$\tau_{ij}^{EV}=-\rho\overline{u_i'u_j'}=\mu_t2S_{ij}-\frac{2}{3}\rho k\delta_{ij}$$

$$CD=\frac{2}{\sigma_\omega}\frac{1}{\omega}\frac{\partial k}{\partial x_j}\frac{\partial\omega}{\partial x_j}$$

$$\tau_{i,j}=\tau_{ij}^{EV}-C_{CORNER}\frac{1.2\mu_t}{max\left(0.3\omega,\sqrt{0.5(S^2+\Omega^2)}\right)}\left(S_{ik}\Omega_{kj}-\Omega_{ik}S_{kj}\right)$$

with

$$S_{ij}=\frac{1}{2}\left(\frac{\partial U_i}{\partial x_j}+\frac{\partial U_j}{\partial x_j}\right)\quad\Omega_{ij}=\frac{1}{2}\left(\frac{\partial U_i}{\partial x_j}-\frac{\partial U_j}{\partial x_{ji}}\right)$$

$$S=\sqrt{2S_{ij}S_{ij}}\;;\;\Omega=\sqrt{2\Omega_{ij}\Omega_{ij}}$$

(2)

2.3. Boundary conditions and solution method

Since the flow considered is compressible, the steady state density-based solver of ANSYS Fluent is used from herein. SIMPLE algorithm is used in the simulation algorithm. The second-order upwind scheme is used for formulating the flow parameters, as well as the turbulent kinetic energy and the dissipation rate. The pressure gradient term is discretized using the least square cell based scheme. Default values of under-relaxation factors as well as the wall function is used in the calculation. The convergence criteria is set at $1 \text{ X } 10^{-7}$.

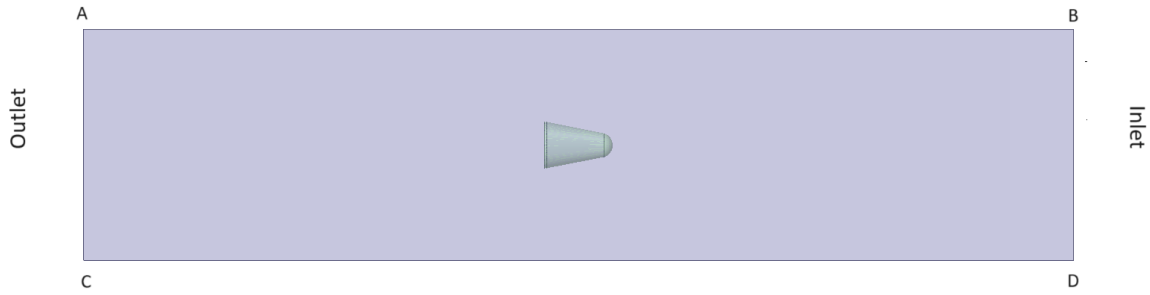

Fig 3: Schematics of the flow in finite domain

In figure 3, the flow domain along with the boundaries for the finite domain has been shown. The no-slip boundary condition is used at the walls AB. CD and the other walls. The inlet velocity, obtained from the Reynolds' number, is specified at the inlet. At the outlet, the gauge pressure is taken to be zero. A no-slip boundary condition is also imposed on the body.

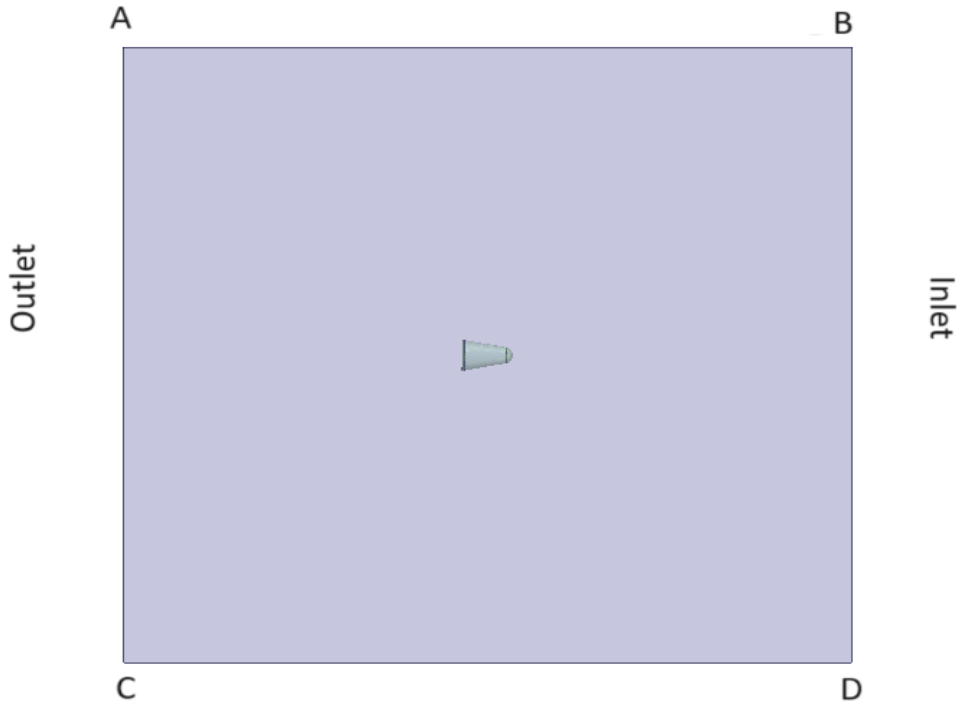

Fig 4: Schematics of the flow in the infinite domain

In figure 4, the flow domain along with the boundaries for the infinite domain has been shown. The symmetry boundary condition is used at the walls AB, CD and the other walls. The inlet velocity, obtained from the Reynolds' number, is specified at the inlet. At the outlet, the gauge pressure is taken to be zero. A no-slip boundary condition is imposed on the body. The symmetry boundary condition imposes a free-slip condition at the walls.

2.4. Mesh independence test

Proper meshing is very important in order to get good results. This is because the selected mesh size affects the results obtained during the simulations. Decreasing the mesh size increases the number of cells which should increase the accuracy of results, but it also increases the computational time. So, a compromise is to be made to find the mesh size which provides good enough results while also not taking too much computational time. Hence mesh independence tests are needed to be performed. To ensure that the meshing done is proper, separate mesh independence tests was conducted for both the finite and infinite domains. For the finite domain, the results of the test with cone 4 have been shown in table 2.

Table 2: Mesh Independence Test for cone 4 in finite domain

Cell size (m)	No. of cells	Drag (N)
0.128	36328	2.2009
0.064	87034	2.2011
0.032	155043	2.2017
0.016	358649	2.20165

It is found from table 2 that there is not much change in going from mesh size of 0.016 m to 0.032 m. So, in order to save computational time, a mesh size of 0.032 m is chosen for finite domain.

Since the infinite fluid domain is supposed to simulate unconfined flow past the body, it is important to ensure that the dimensions of the cross-section of the infinite domain is large enough so that the drag computed is actually close to the drag obtained for unconfined flow. So, the cross-section of the infinite domain is chosen such that the drag obtained is not changing even after increasing the dimensions of the cross-section. These results have been shown below.

Table 3: Mesh Independence Test for cone 4 in infinite domain

Domain Cross-section	Mesh size (m)	No of elements	Drag(N)
1 m X 1 m	0.25	15123	2.065286
	0.125	35333	2.078581
	0.0625	81056	2.095575
	0.03125	174356	2.095867
2 m X 2 m	0.25	28945	2.145221
	0.125	46253	2.112360
	0.0625	118961	2.1045126
	0.03125	256154	2.1045369
4 m X 4 m	0.25	38256	2.111301
	0.125	69256	2.101590
	0.0625	159719	2.109312
	0.03125	356982	2.109300
8 m X 8 m	0.25	45174	2.111302
	0.125	91278	2.101821
	0.0625	375682	2.109120
	0.03125	611958	2.109121

It can be seen from table 3 that there is very little difference in the drag values obtained when the cross-section area is changed from 4 m X 4 m to 8 m X 8 m. So, the dimensions of the infinite domain have been taken to be 4 m X 4 m. Also, there is even smaller difference between drag measured for mesh sizes 0.0625 m to 0.03125 m. Hence, in order to save computational time, the mesh size is chosen to be 0.0625 m for the infinite domain.

To find the suitable mesh size for simulating the effects of the presence of measurement system, a separate mesh independence test was performed for cone

1 mounted on the measurement system. These results have been shown in table 4.

Table 4: Mesh Independence Test for cone 1 mounted on a supporting system

Cell Size (m)	No of elements	Drag (N)
0.128	38345	0.1322
0.064	88654	0.1412
0.032	159324	0.1499
0.028	181234	0.1515
0.016	365267	0.1518

From table 4, it is clear that the drag computed does not vary significantly between the mesh sizes of 0.028 m and 0.016 m. So, to reduce computational time, the mesh size of 0.028 m was chosen.

The enlarged view of the mesh for both finite and infinite domains and the cones with supporting system have been shown in figures 5,6 and 7.

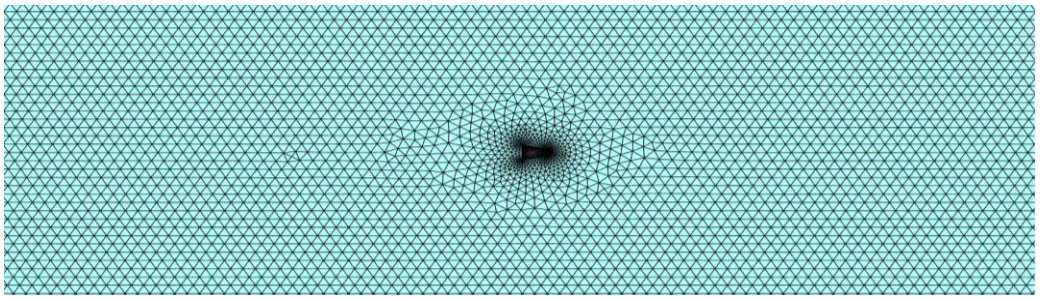

(a)

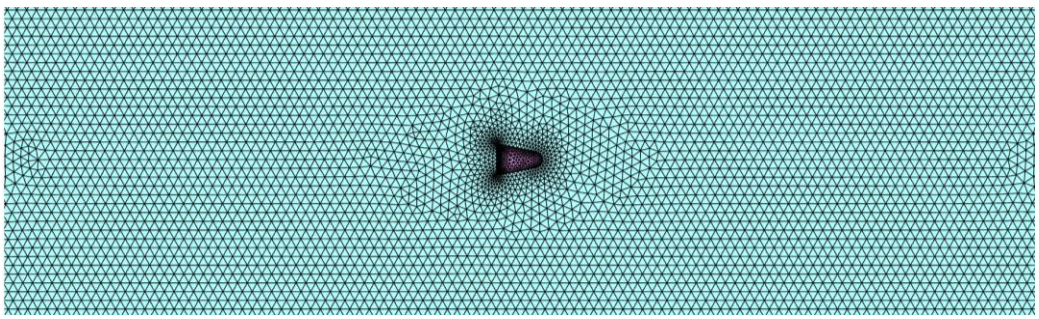

(b)

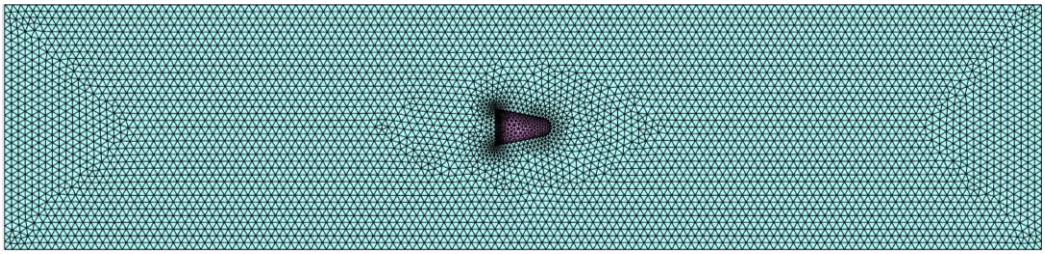

(c)

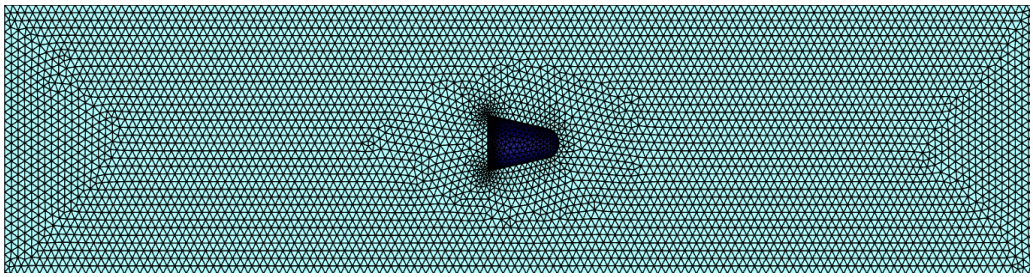

(d)

Fig 5: Enlarged view of the generated mesh for finite domain for (a) Cone 1, (b) Cone 2, (c) Cone 3 and (d) Cone 4

From figures 5, 6 and 7, it can be seen that the mesh generated consists of unstructured grids, particularly around the body. However, far away from the body, the mesh is comprised of well structured grids.

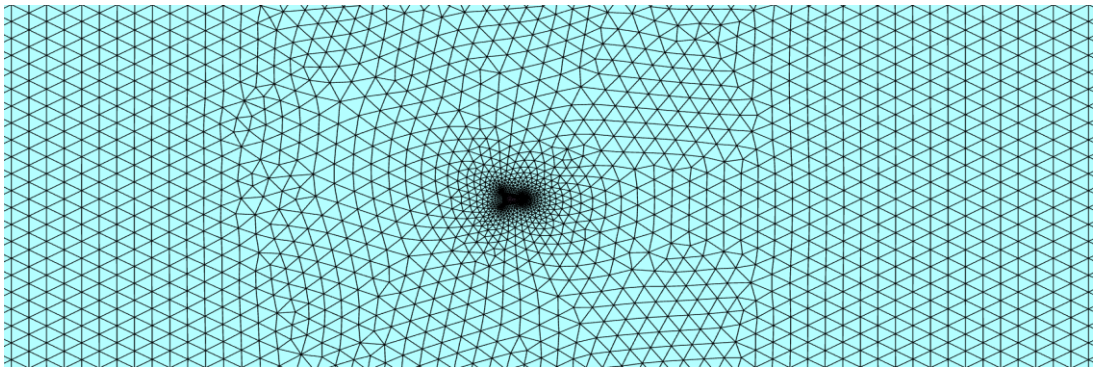

(a)

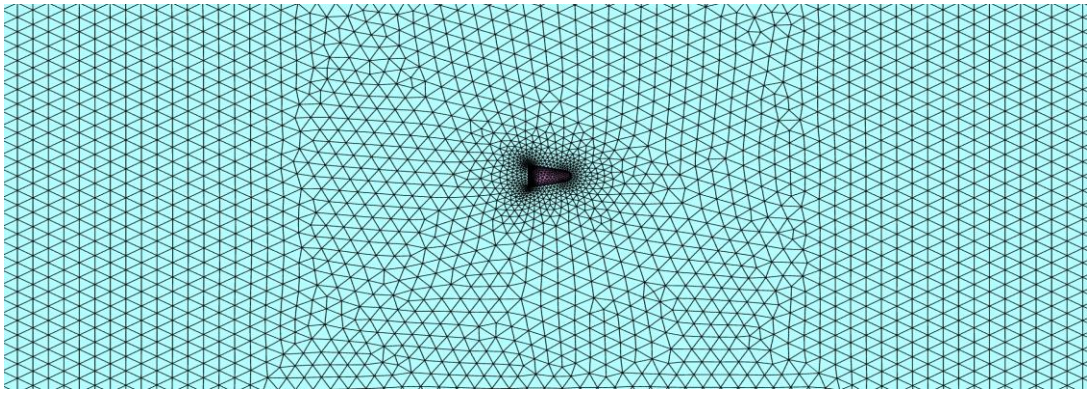

(b)

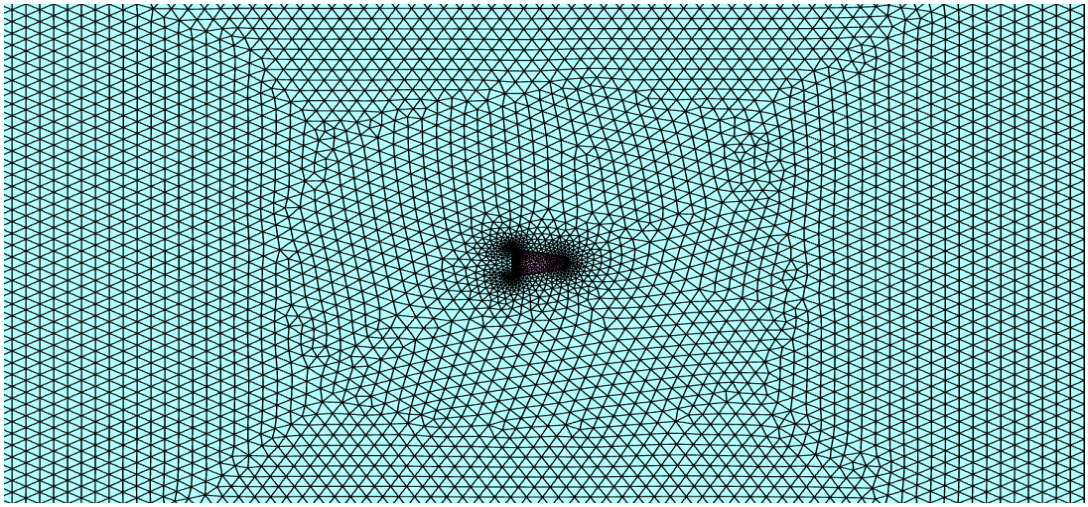

(c)

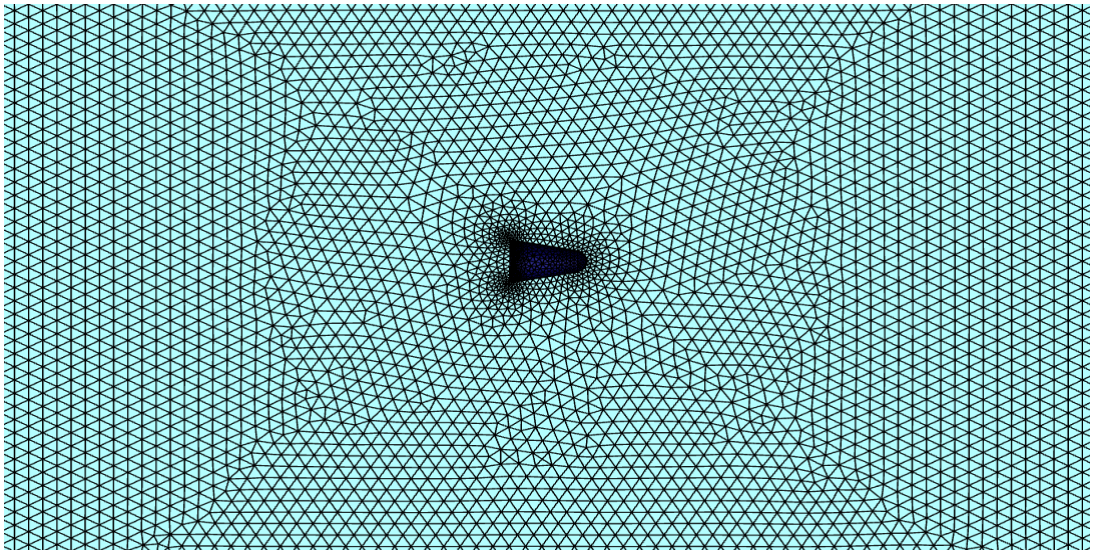

(d)

Fig 6: Enlarged view of the generated mesh for infinite domain for (a) Cone 1, (b) Cone 2, (c) Cone 3 and (d) Cone 4

The following figure shows the generated mesh for the case in which the body is mounted on a supporting system.

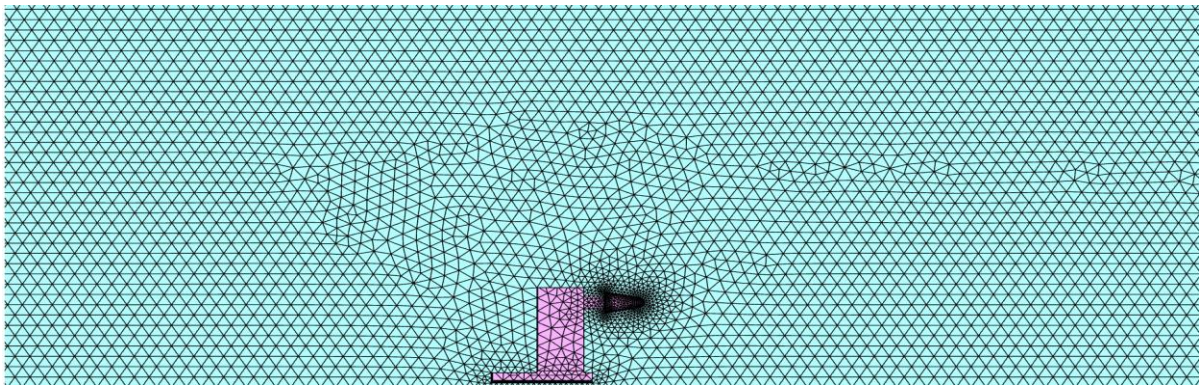

(a)

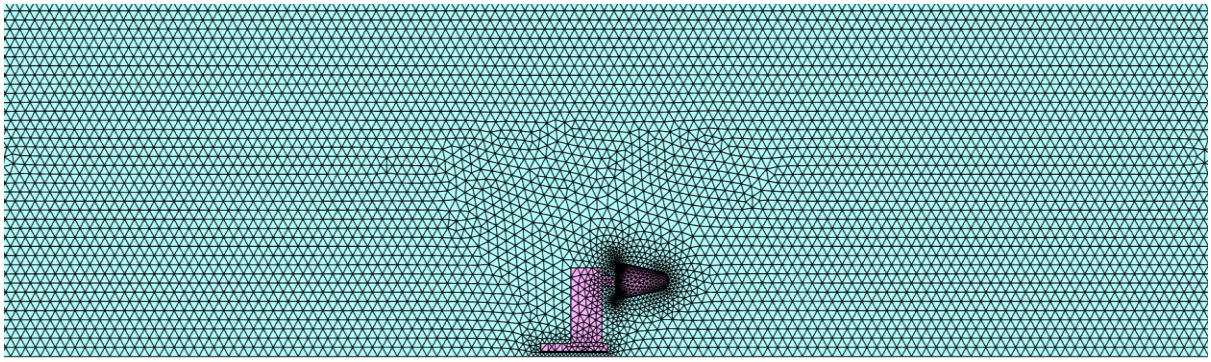

(b)

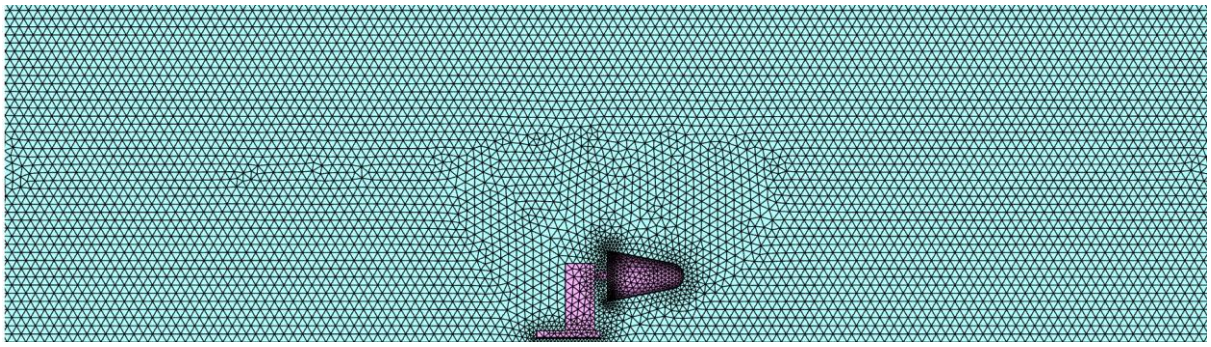

(c)

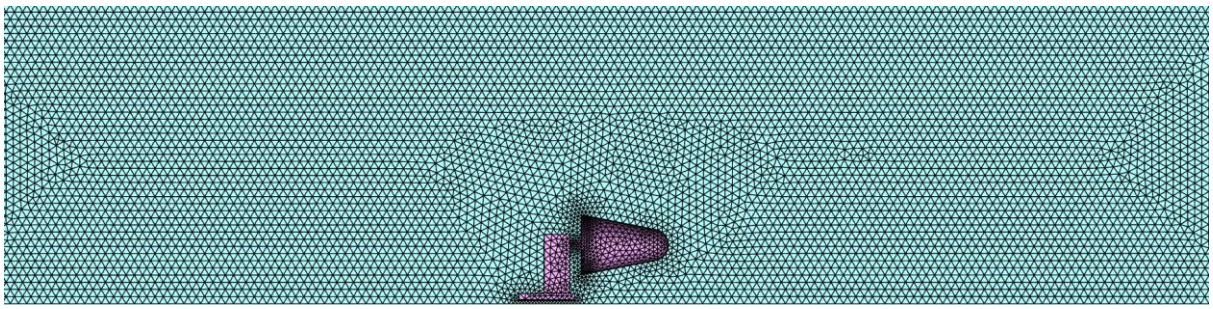

(d)

Fig 7: Enlarged view of the generated mesh for (a) cone 1, (b) cone 2, (c) cone 3, (d) cone 4 with supporting system

2.5. Validation of Results

In the present study, the effect of tunnel interference and blockage ratio on the drag on a conical bluff body has been depicted. However, before presenting the results, it is imperative to validate the method of calculation of this work with some other established research. Unfortunately, there is very limited information on this topic in literature. The study conducted in [28] and more recently in [29] seem to be two of the very few pieces of literature that describe the effects of blockage ratio on the coefficient of drag of a conical body that has achieved terminal velocity whilst falling through a fluid, which is very close to the matter discussed in this thesis. Hence, this work's result can be safely validated against the works mentioned above. For performing the said validation, the cone size (d= 0.005 m, l = 0.0058 m) was chosen such that the blockage ratio was exactly the same as the cone 2 used by Sharma and Chhabra. The cross-section of the infinite domain used was 4 m X 4 m.

Sharma and Chhabra [28] experimentally obtained the values of C_D against a few Reynolds' numbers (Re) and found an equation describing their relationship. This equation is given as

$$C_D = \frac{17}{Re}(1 + 0.19Re^{0.805}) \quad (3)$$

Samantaray et. al**.** [29] found similar results numerically. A comparison of their data with that of this work has been given herein.

The mesh size used is 0.032 m.

Table 5: Validation of results

Re	Expt. C_D by Sharma and Chhabra	C_D from Samantaray et. al.	C_D from this work
134.2618	1.368991	1.4882	1.4766
224.9749	1.016599	1.09872	1.0202
455.0123	1.198969	1.2878	1.2012

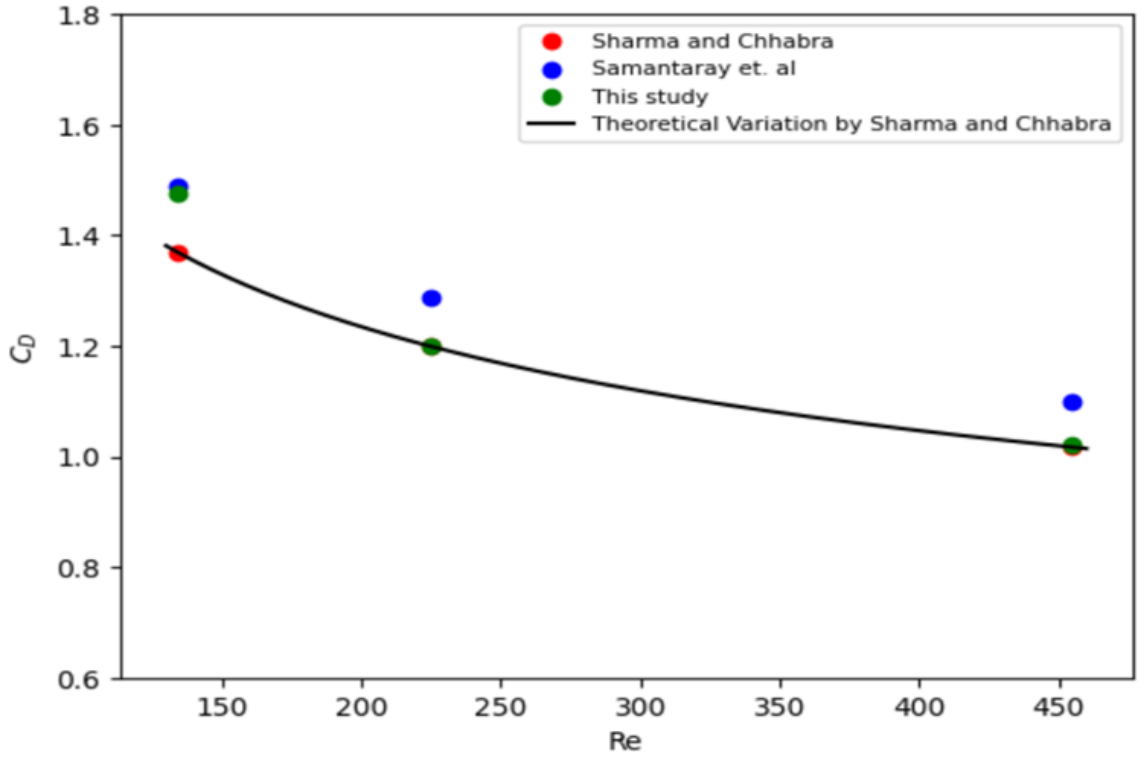

Fig 8: Plot comparing C_D vs Re for [28], [29], and this work

The figure 8 shows excellent agreement between equation (4) and this work. The results get closer with the increase in Reynolds' number.

Chapter 3:

Results and Discussions

In this section, the effect of tunnel interference and supporting system interference on coefficient of drag on a conical bluff body for both confined and unconfined flows have been depicted. The confined flow has been modelled using the "finite" fluid domain, whereas the unconfined flow has been modelled using the "infinite" fluid domain. For both of these domains, a square cross-section has been chosen. The cross-section of the finite domain is chosen to be 1 m X 1 m, while that for the infinite domain has been chosen to be 4 m X 4 m.

The coefficient of drag is calculated as usual, and is given by

$$C_D = F_D / (\frac{1}{2}\rho_\infty U^2 A_p) \quad (4)$$

where, ρ_∞ is the free stream density, F_D is the drag force, U is the velocity of air at the inlet and A_p is the projected area of the body. In our case, $A_p = \frac{\pi d^2}{4}$, where d is the diameter of the base of the conical body. So, for our case, equation (4) can be re-written as

$$C_D = \frac{8\, F_D}{\pi U^2\, d^2 \rho_\infty} \quad (5)$$

The projected area has been taken to be the base circle's area because the flow considered is axial.

Even though the body has a circular cross-section, the cross-section of the finite fluid domain has been chosen to be square so as to simulate the conditions that arise during a wind tunnel testing.

3.1. Effect of blockage ratio on coefficient of drag

The blockage ratio (β) is defined as the ratio of the area of cross-section of the model to the cross-section area of the wind tunnel walls. Since the finite domain is meant to represent the wind tunnel walls, so, in our case, the blockage ratio is given as

$$\beta = \frac{\pi\, d^2}{4\, A_T} \quad (6)$$

where A_T is the cross-section area of the finite domain.

Figure 9 shows the variation of the coefficient of drag with Reynolds' number for different values of blockage ratios for the finite domain.

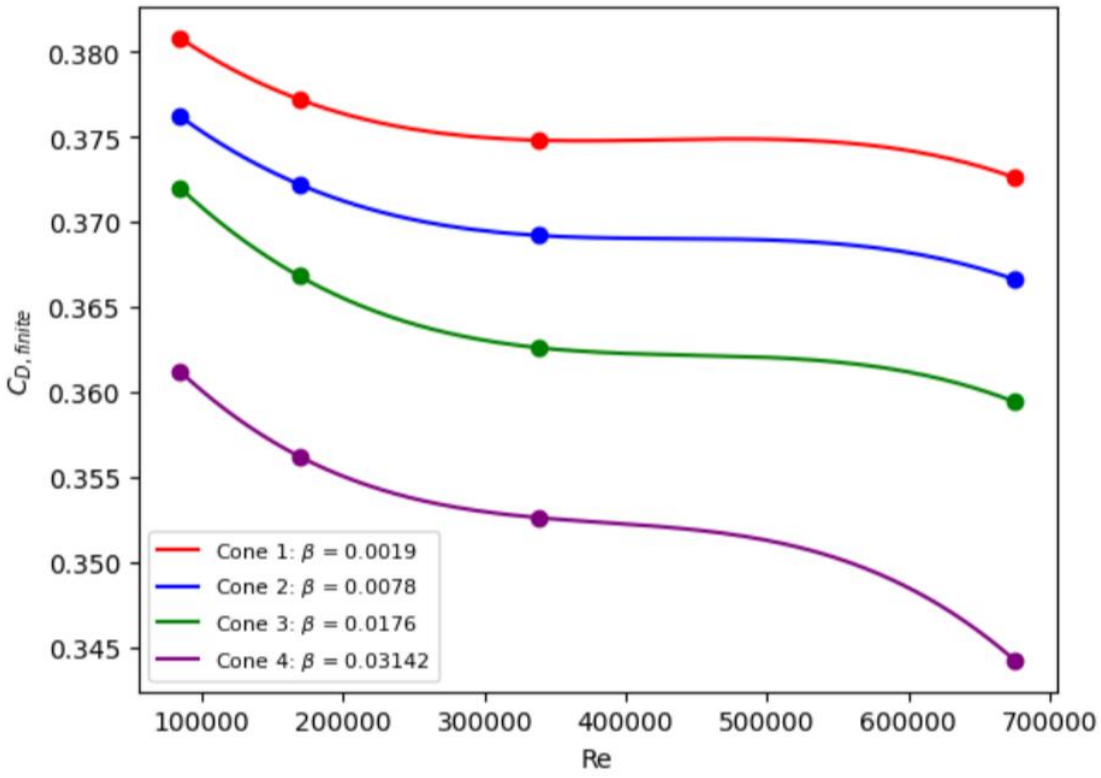

Fig 9: C_D vs Re for confined flow for different values of β

From figure 9, it is clear that the coefficient of drag decreases with increase in Reynolds' number for both confined and unconfined flows, which is consistent with the findings of Samantaray et. al. and Sharma et. al. It is to be noted though, that the drag force on the body increases with an increase in the Reynolds' number, but the dynamic pressure increases much faster with Reynolds' number, and the drag coefficient decreases. From figure 1, it can also be noted that the drag coefficient also decreases with increase in blockage ratio, for the same Reynolds' number.

3.2. Effect of tunnel interference on measurement of drag

From the simulations that have been conducted, it is found that for all the Reynolds' numbers and blockage ratios, the drag force on the same model is larger for confined flow than for unconfined flow, which is the expected result. In the confined flow, the tunnel interference is responsible for increasing the drag force on the model. Hence the drag force measured in the confined flows are spurious to some extent. So, an error in drag has been defined as

Percentage error in drag = $(D_{finite}-D_{infinite})/D_{infinite}\ X\ 100$ (7)

where D_{finite} is the drag force measured in the confined domain and $D_{infinite}$ is that measured in the unconfined domain.

The following figure shows the difference in the values of drag coefficients between the confined and unconfined flows for different blockage ratios.

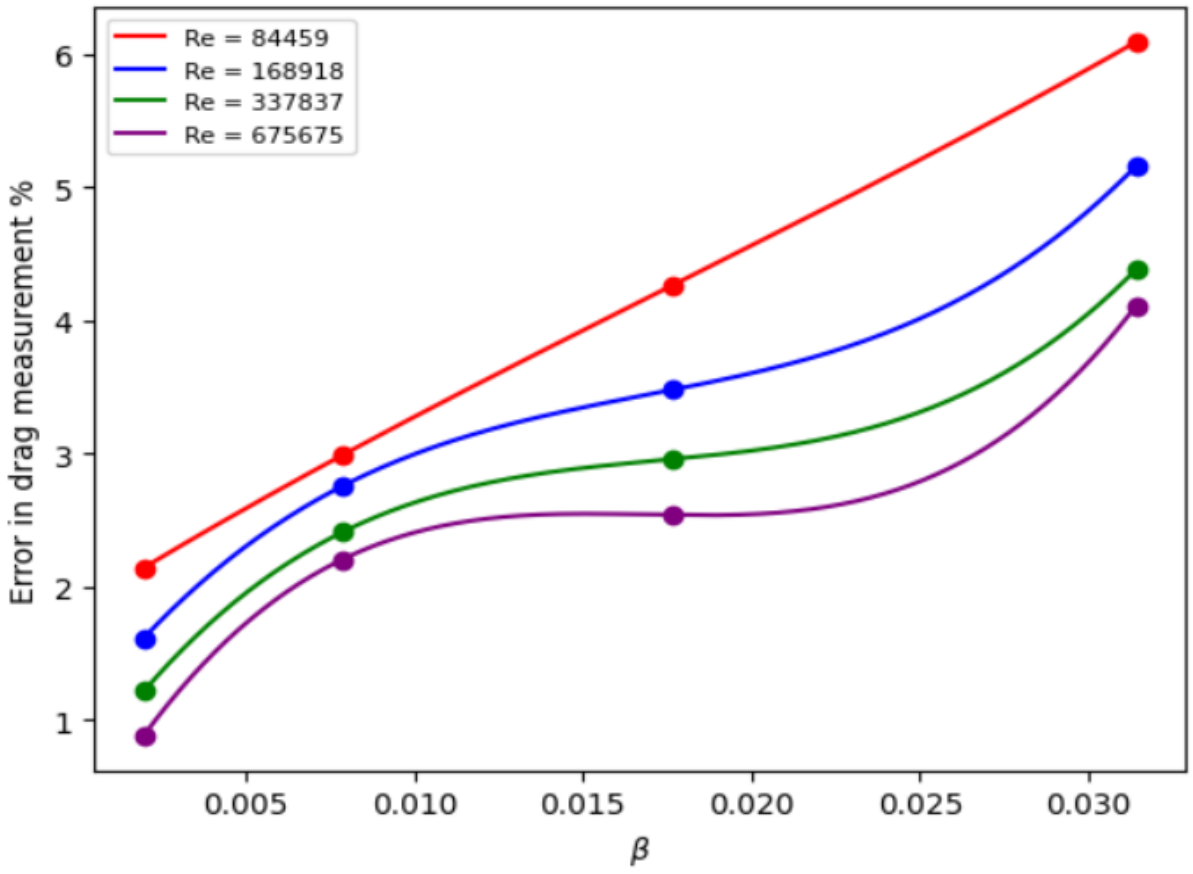

Fig 10: Percentage Error in measured drag vs β for different Re

From figure 10, it is clear that the percentage error in drag increases with an increase in blockage ratio at all Reynolds' numbers. This is because, at higher blockage ratios, the effect of tunnel interference is more pronounced. As a result, there is a larger error in the measured drag and hence a larger error percentage. It can also be seen from figure 2 that this error percentage decreases with an increase in the Reynolds' number. In this case, while the error in drag increases when increasing the Reynolds' number, the value of $D_{infinite}$ increases much more quickly with Reynolds' number and hence the error percentage decreases.

The following figure shows the effect of Reynolds' number on the error of drag measurement. The quantity $C_{D,error}$ has been defined as

$$C_{D,error} = C_{D,finite} - C_{D,infinite} \quad (8)$$

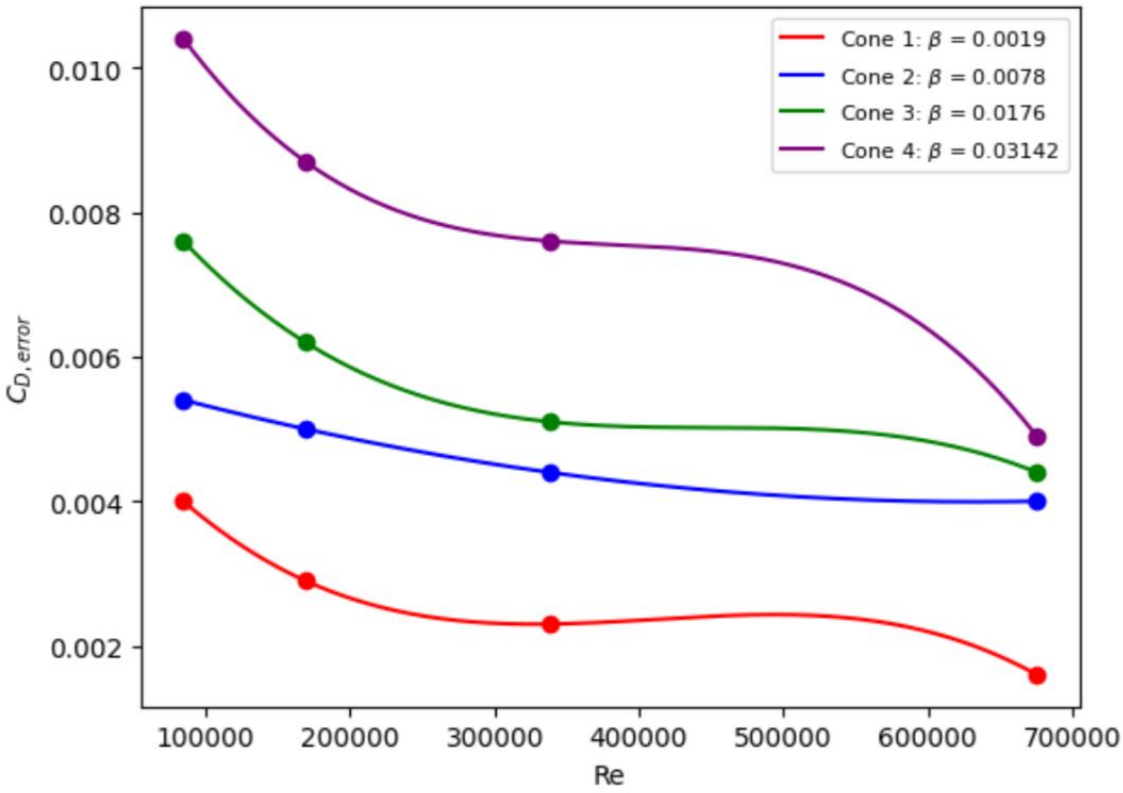

Fig 11: $C_{D,error}$ vs Re for different blockage ratios

From figure 11, it can be seen that the value of $C_{D,error}$ decreases with an increase in Reynolds' number.

From the discussion up till now, it is clear that the tunnel interference significantly affects the drag coefficient that is measured during the wind tunnel testing. Since

there exists a developing flow within the tunnel walls, the core velocity is higher than the velocity at inlet. Hence, the stagnation pressure on the front surface is higher for confined flow than what should be for the unconfined flow. This increases the pressure drag on the body. Moreover, the rigid boundaries of the tunnel walls prevent a free lateral displacement of the fluid stream caused by the body. This causes the streamlines of the flow to converge in the neighbourhood of the body and the velocities become greater than what they would have been in an unconfined stream. Thus, the velocity gradients in the vicinity of the body become greater than that in an unconfined flow and this causes the skin friction drag to increase in the confined flow. All of these effects cause the total drag to increase in the case of confined flow.

The following figures make the above effects clear.

(a)

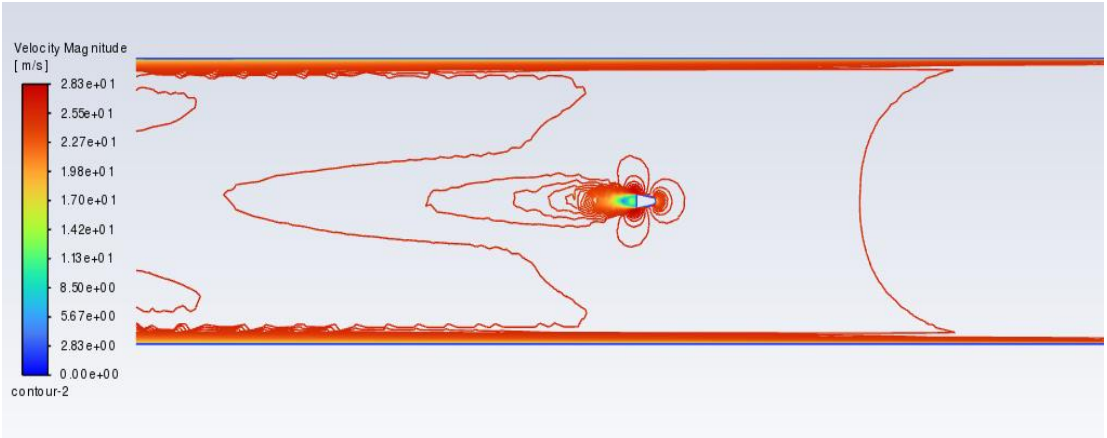

Finite

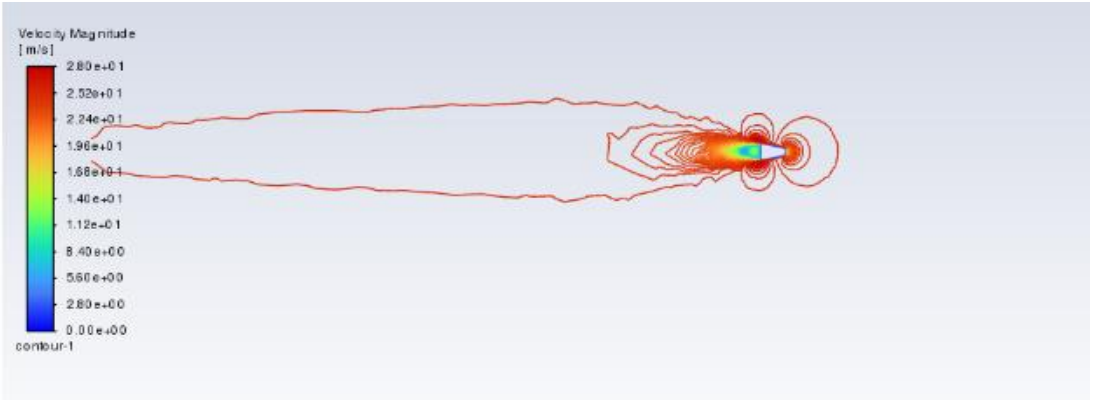

Infinite

(b)

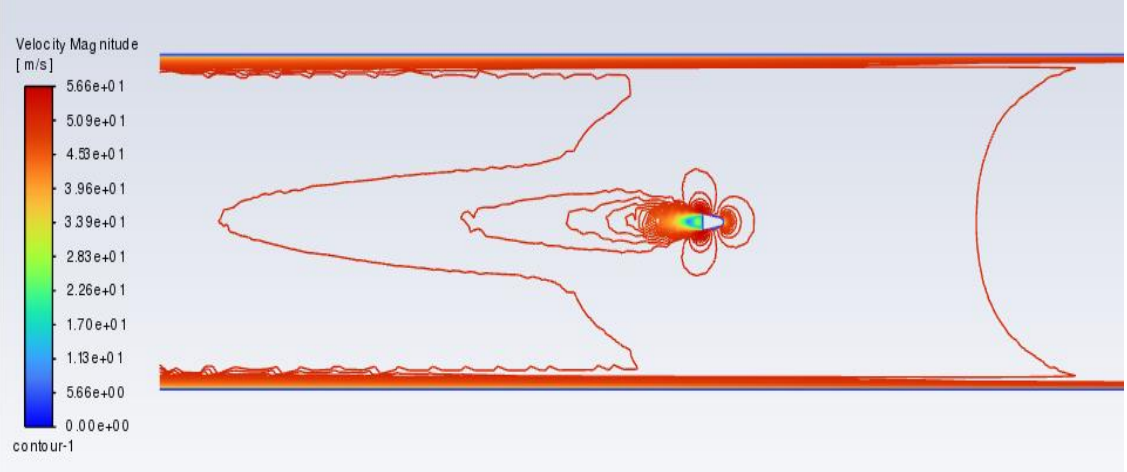

Finite

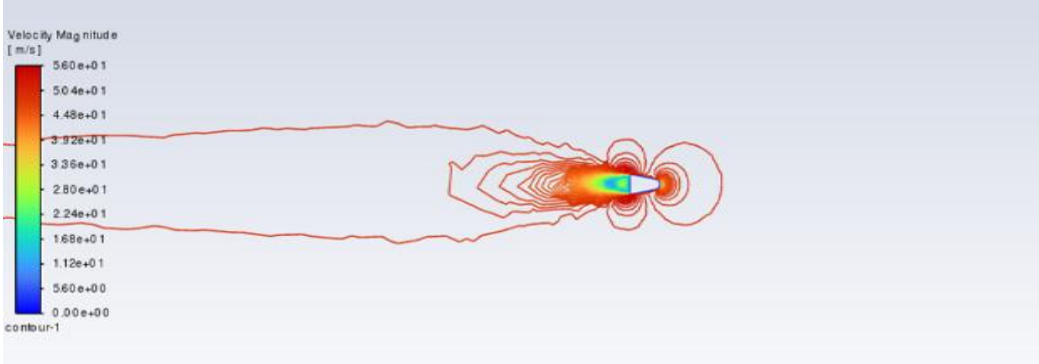

Infinite

(c)

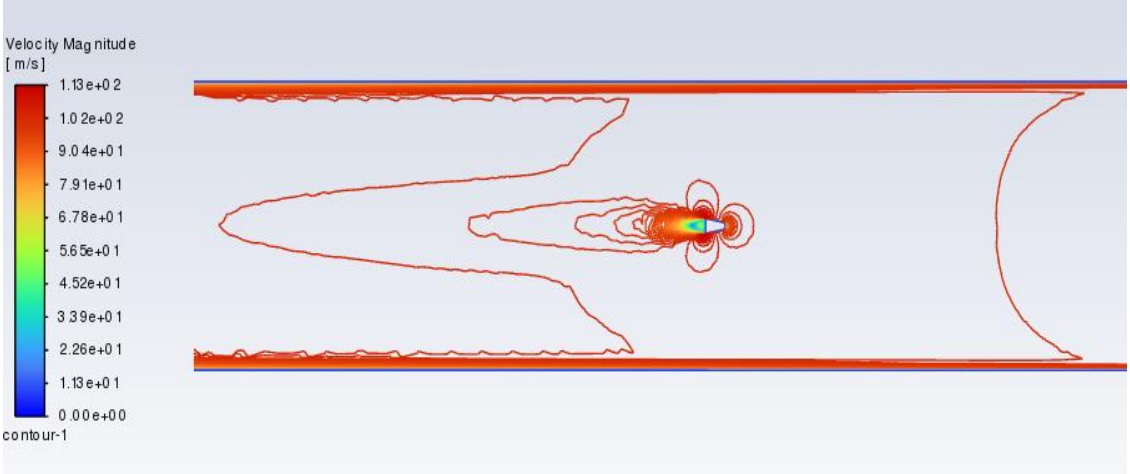

Finite

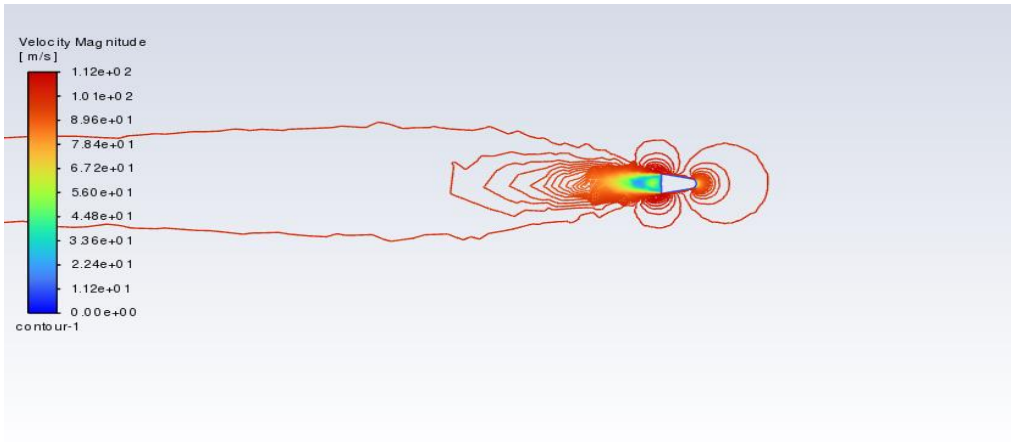

Infinite

(d)

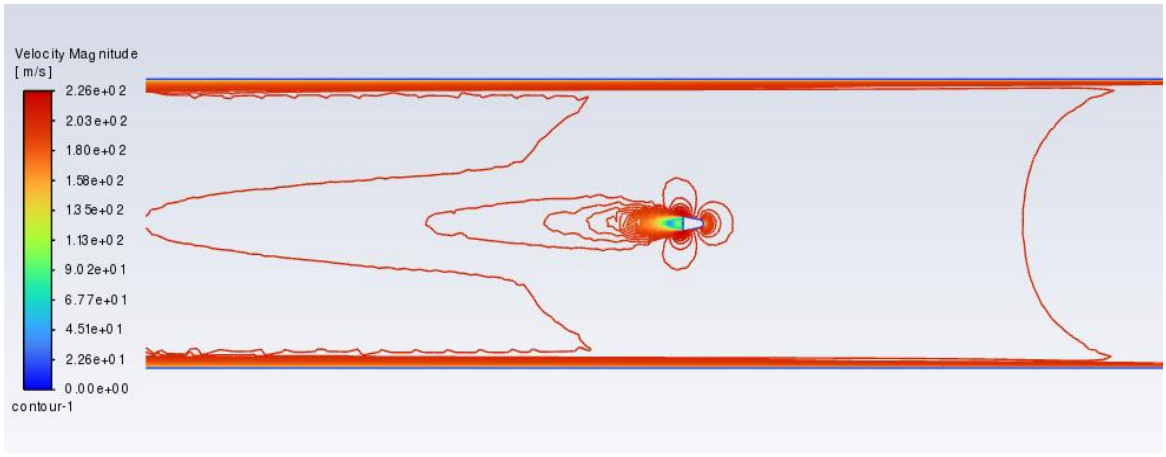

Finite

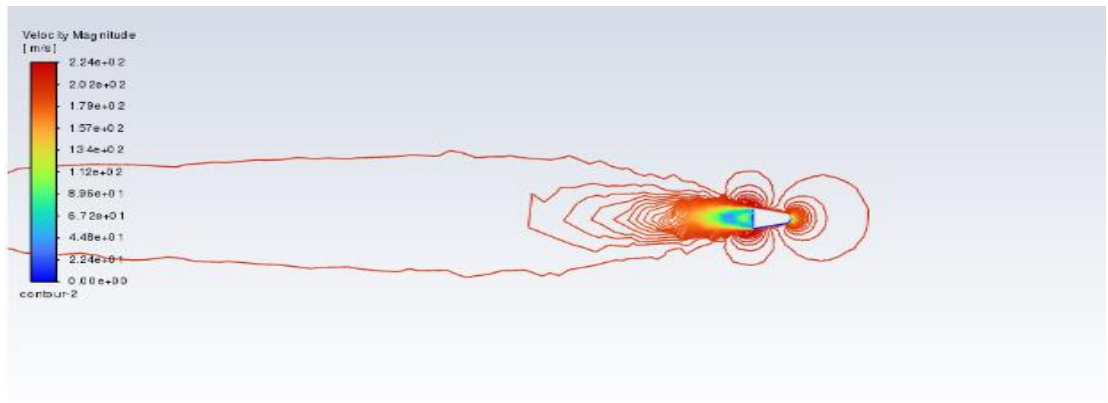

Infinite

Fig 12: Velocity Contours for cone 1 both finite and infinite domains for (a) Re = 84459, (b) Re = 168918, (c) Re = 337837, (d) Re = 675675

From figure 12, it can be seen that for cone 1 there is not much of a difference in the velocity contours for finite and infinite domains. Most of the difference lies

in the downstream of the body. This suggests that the interference from the boundary layers on tunnel walls is not significant. This is reflected in figure 10 and 11 where the error in drag coefficient is the least for cone 1 at all Reynolds' numbers.

(a)

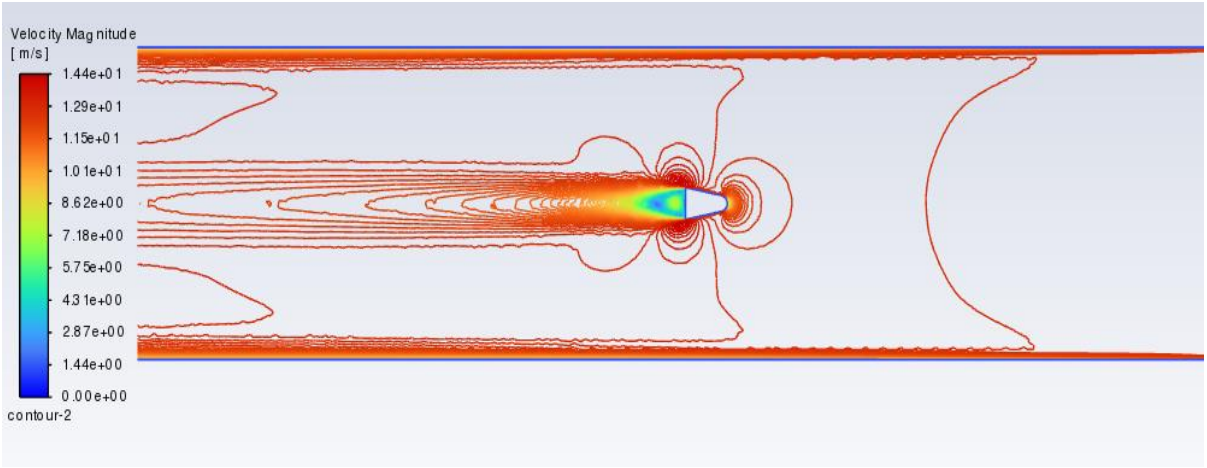

Finite

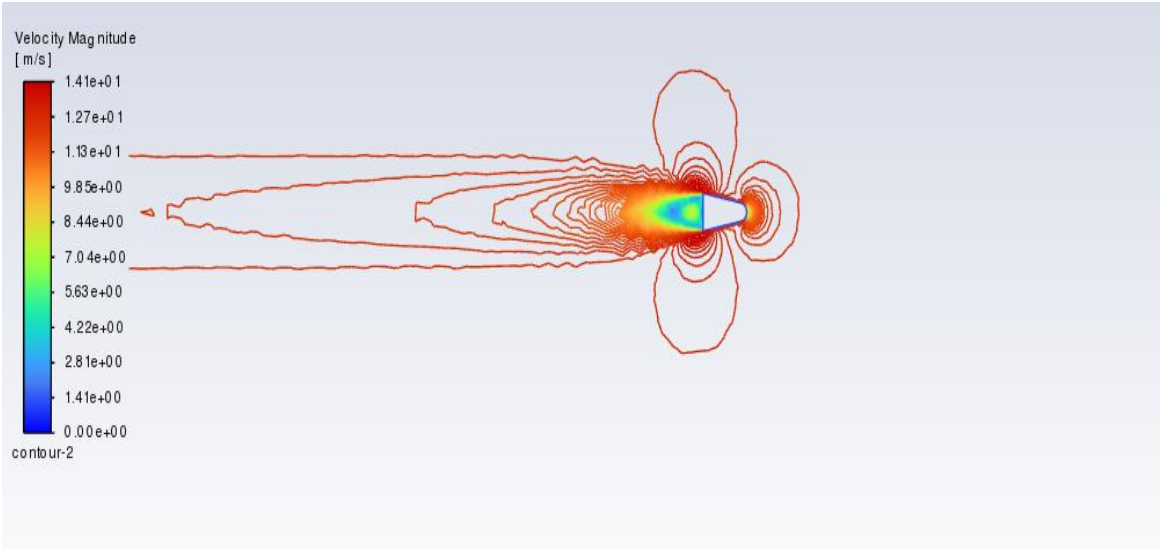

Infinite

(b)

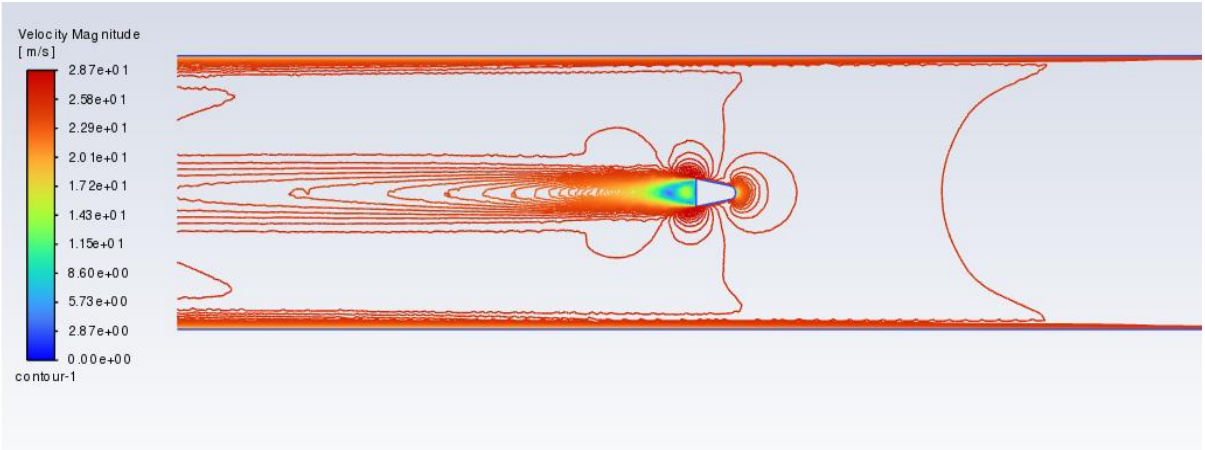

Finite

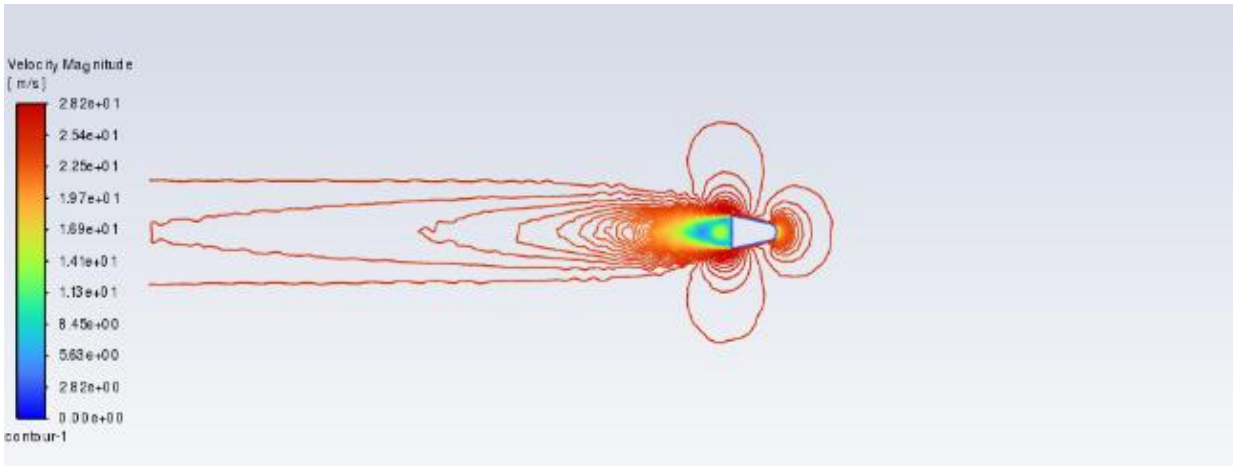

Infinite

(c)

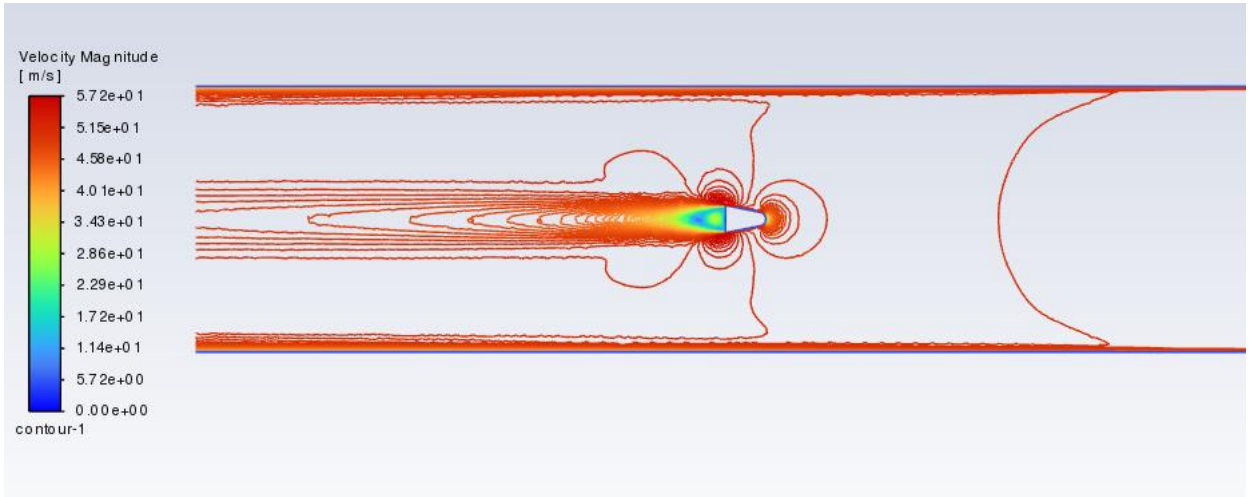

Finite

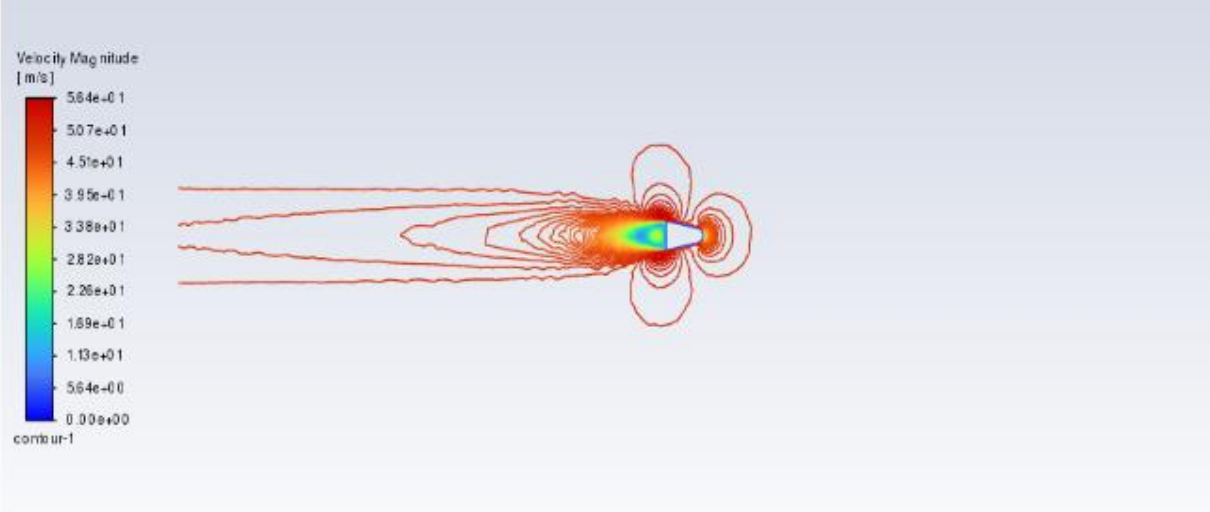

Infinite

(d)

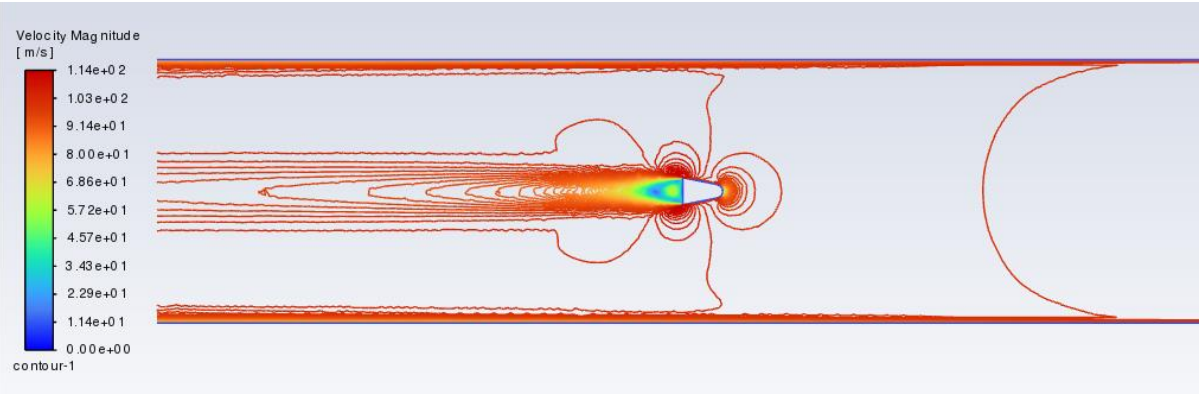

Finite

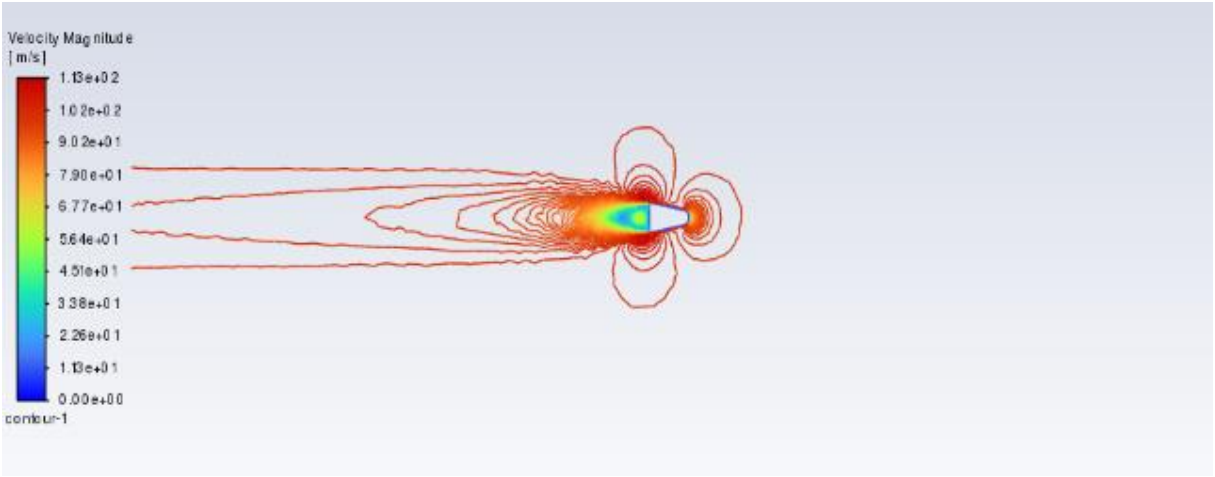

Infinite

Fig 13: Velocity Contours for cone 2 both finite and infinite domains for (a) Re = 84459, (b) Re = 168918, (c) Re = 337837, (d) Re = 675675

From figure 13, it can be seen that for cone 2 there are a few differences in the velocity contours between the finite and infinite domains. The boundary layers

on the tunnel walls interact with the flow field and alter the flow field around the body. This implies a slightly larger tunnel interference effect and slightly larger error while measuring drag, than it was for cone 1. This too is reflected in figures 10 and 11.

(a)

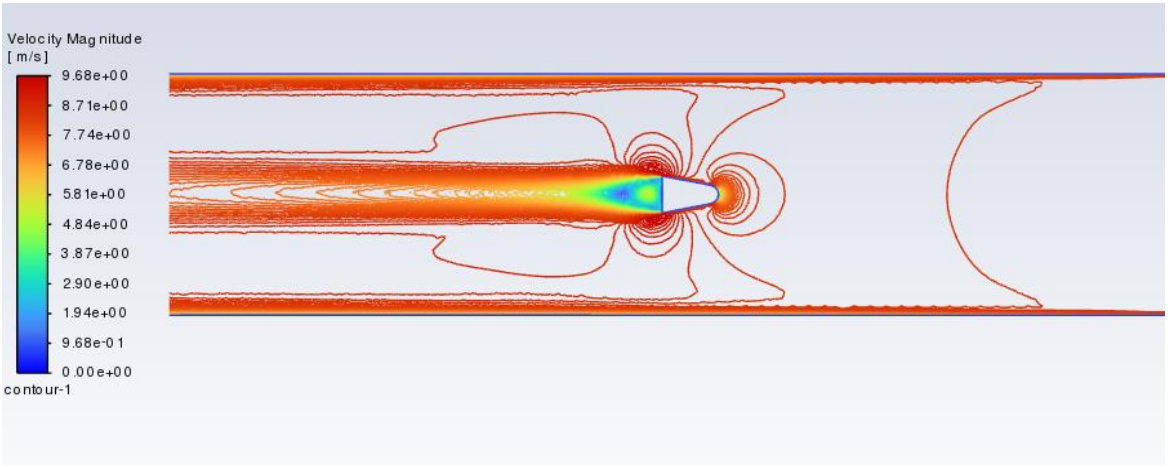

Finite

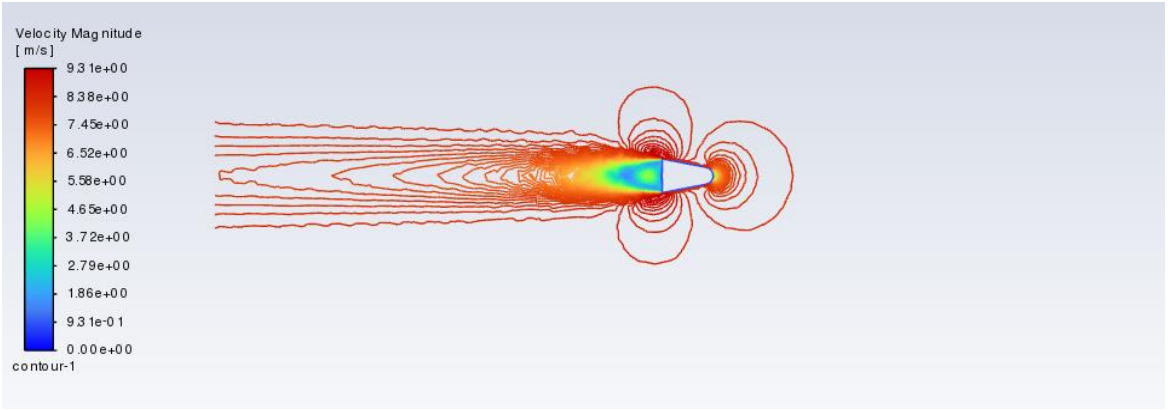

Infinite

(b)

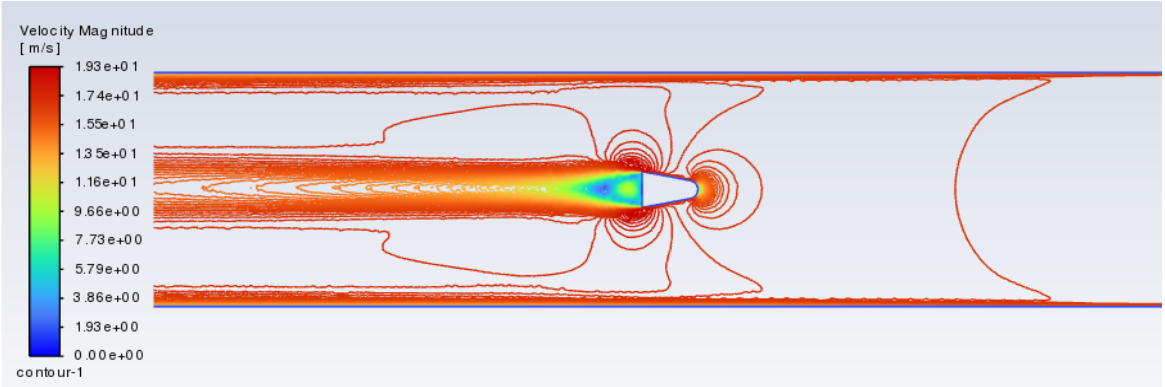

Finite

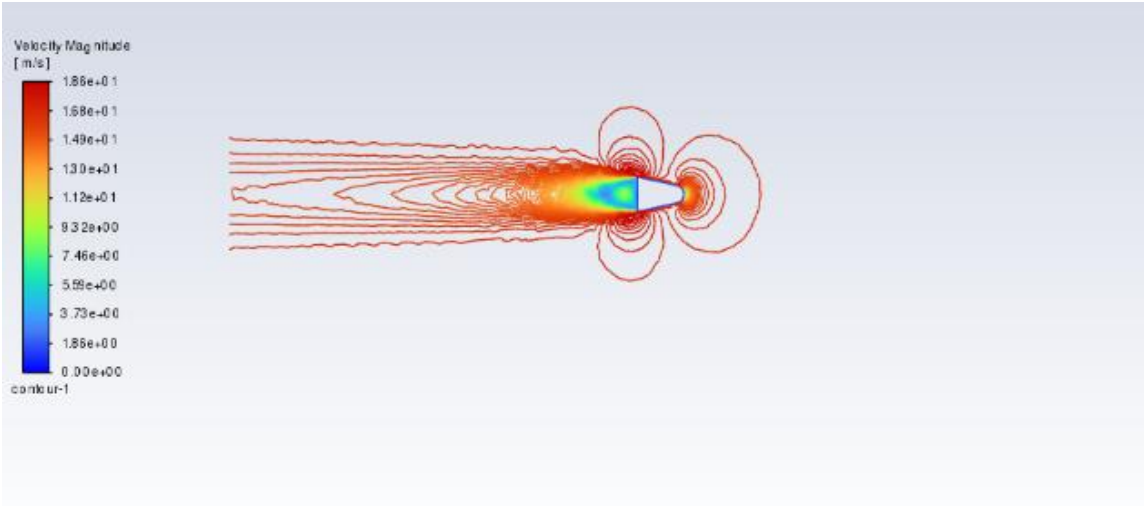

Infinite

(c)

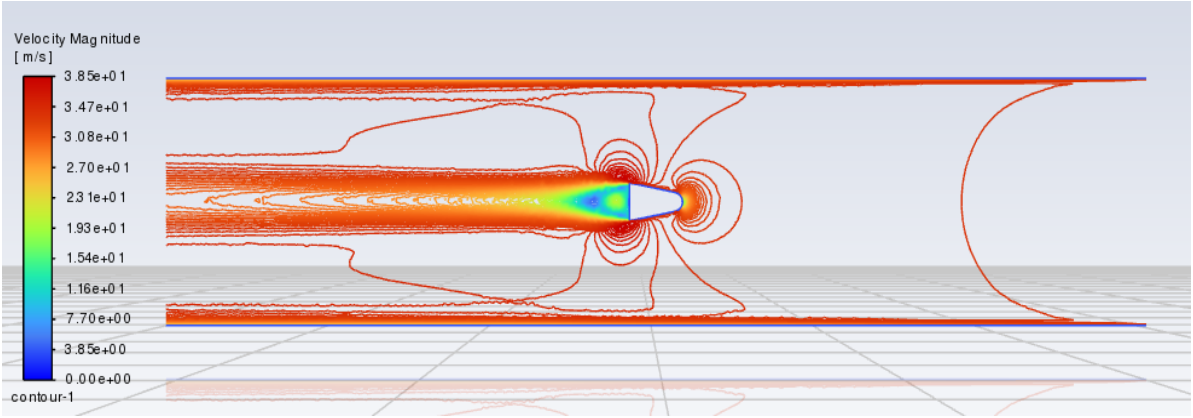

Finite

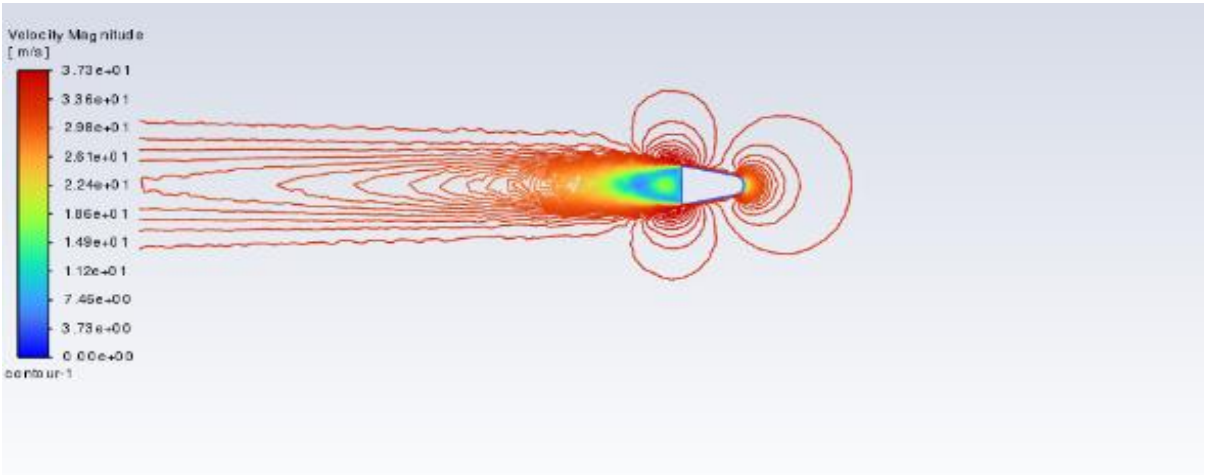

Infinite

(d)

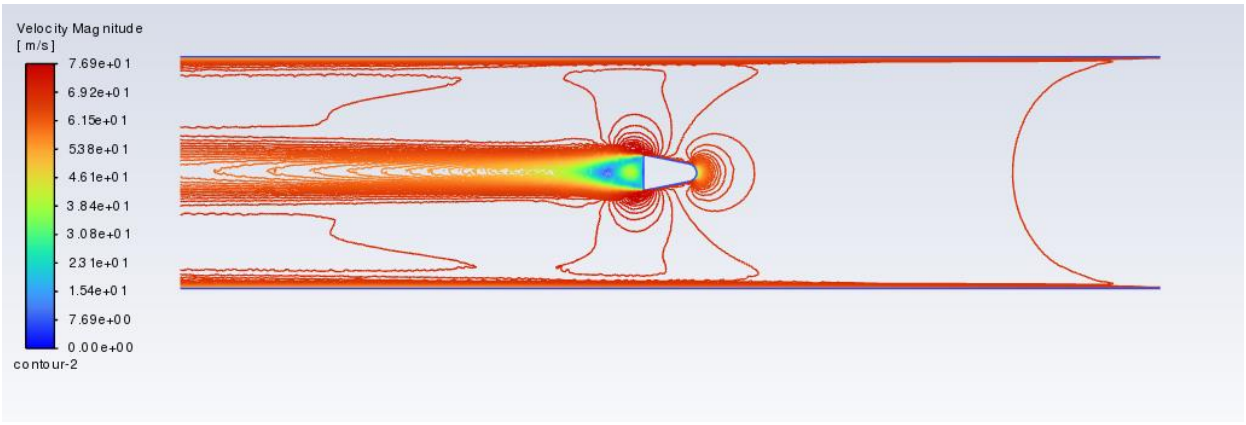

Finite

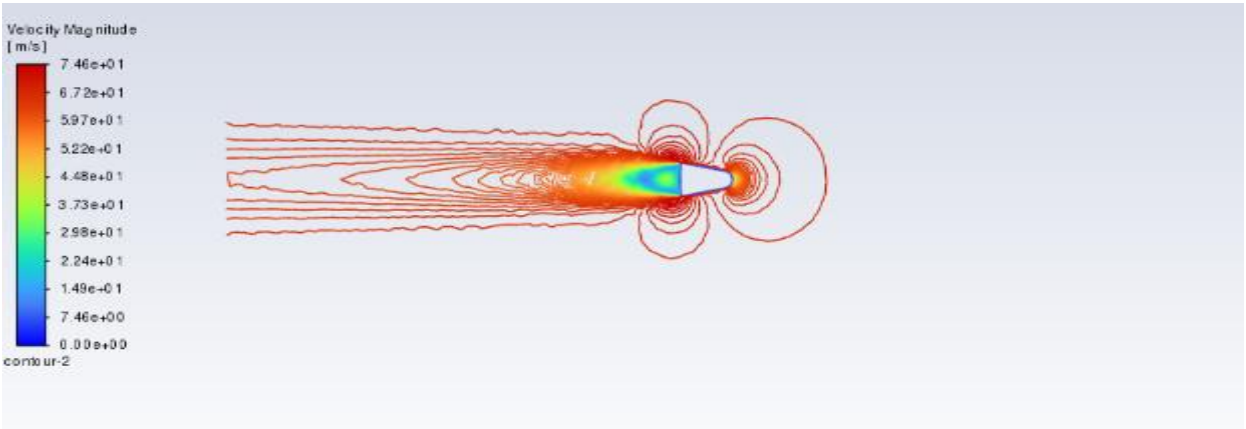

Infinite

Fig 14: Velocity Contours for cone 3 both finite and infinite domains for (a) Re = 84459, (b) Re = 168918, (c) Re = 337837, (d) Re = 675675

From figure 14, we can see that for cone 3 the interference of tunnel wall boundary layers on the flow field for confined flow is significant. The velocity contour lines in the vicinity of the body in confined flow are much closer to each other than in the unconfined flow. This shows that the velocity gradients are much larger in the confined flow than for the unconfined flow. This indicates that the error in drag measurement shall be higher for cone 3 than for both cones 1 and 2. This is clearly depicted in figures 10 and 11.

(a)

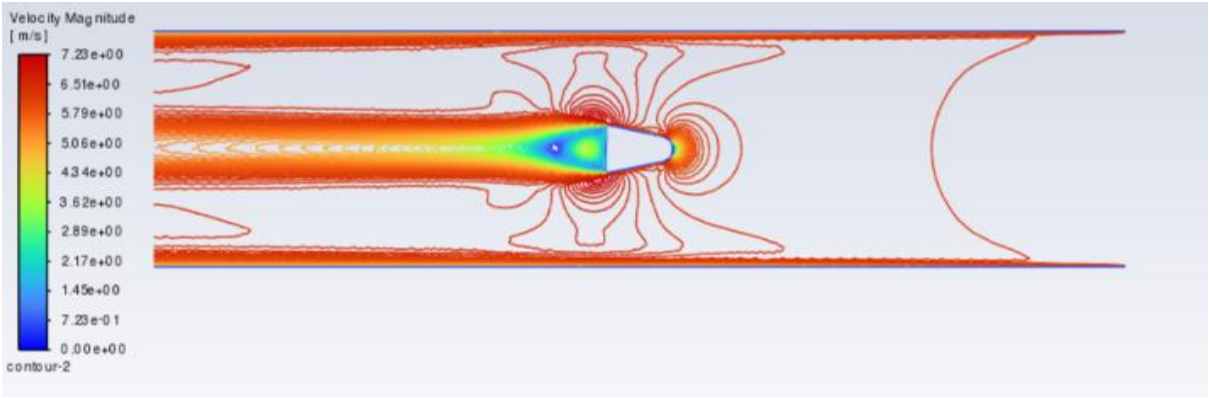

Finite

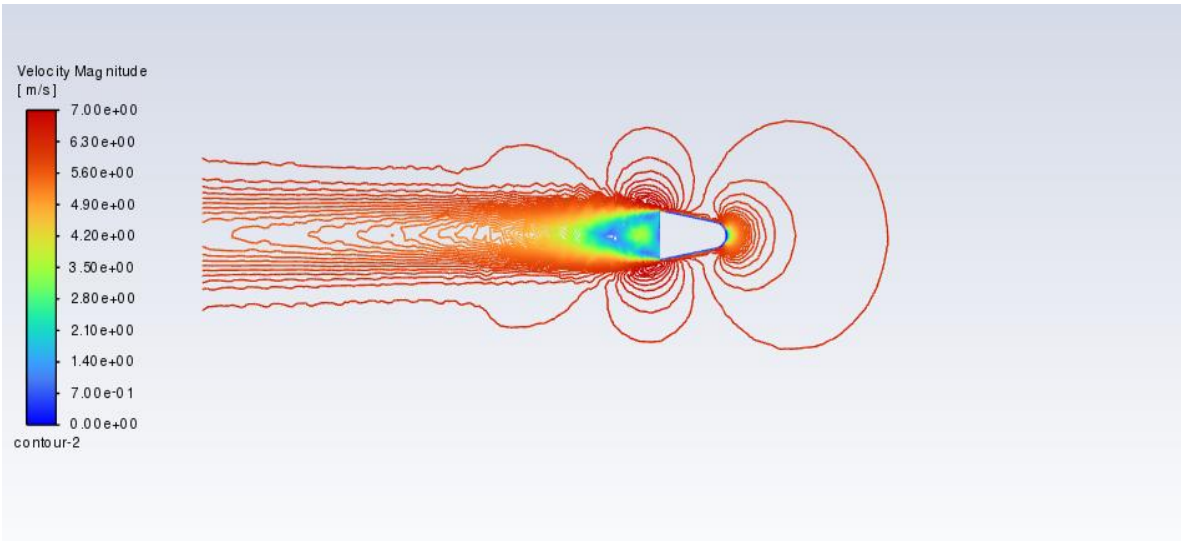

Infinite

(b)

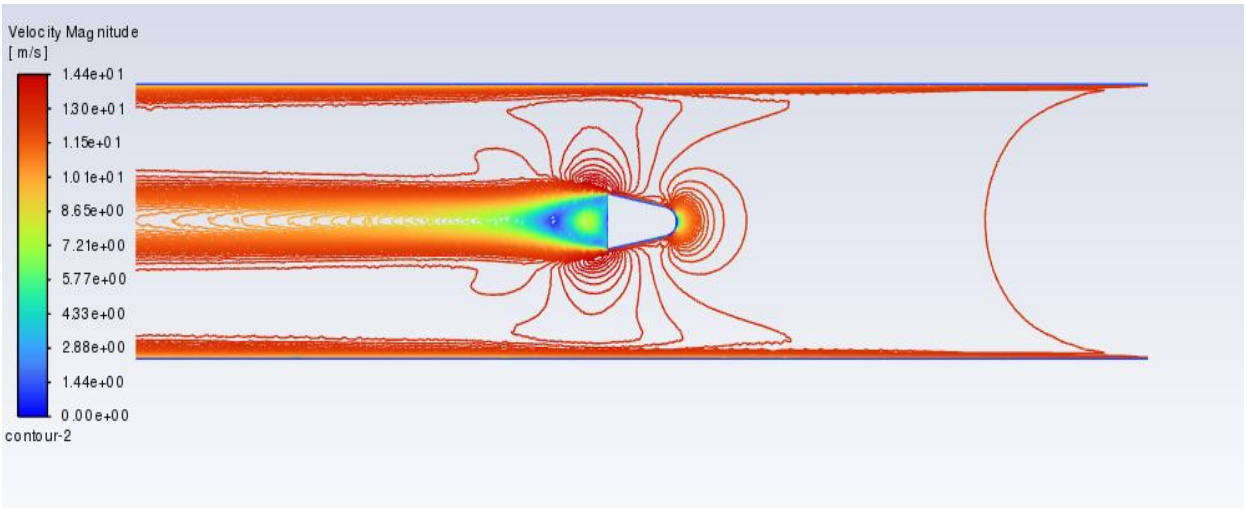

Finite

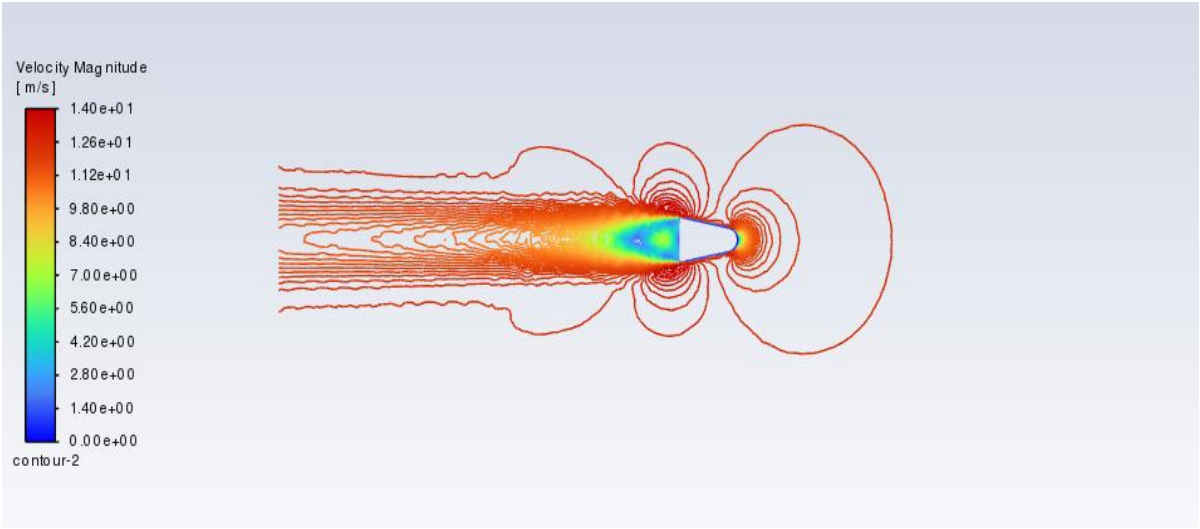

Infinite

(c)

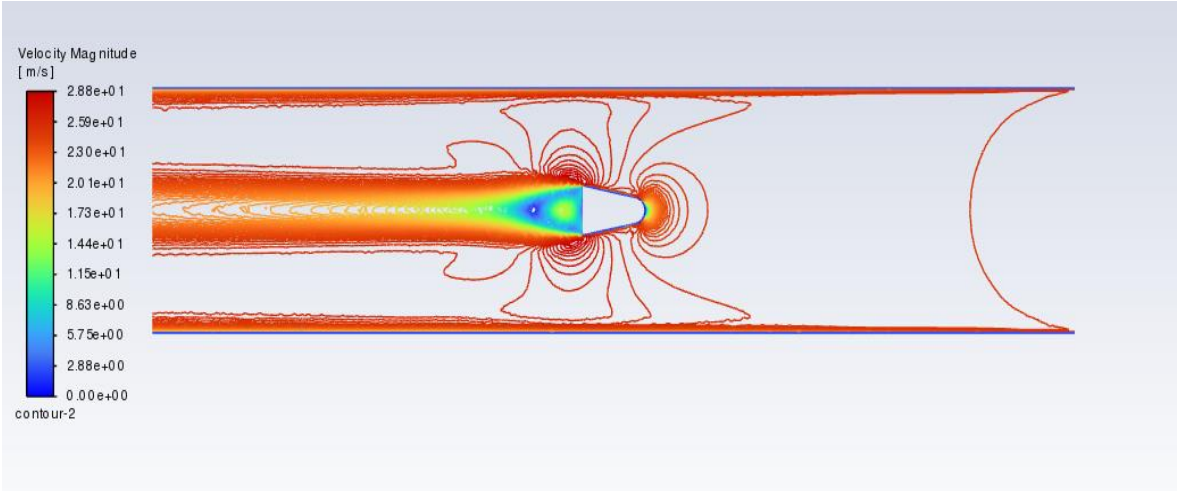

Finite

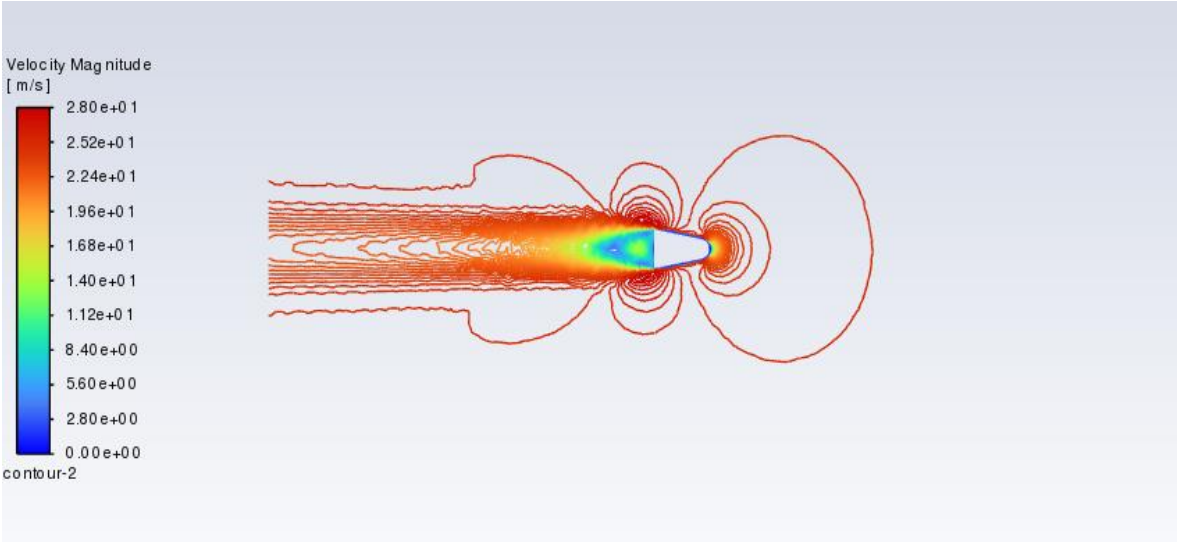

Infinite

(d)

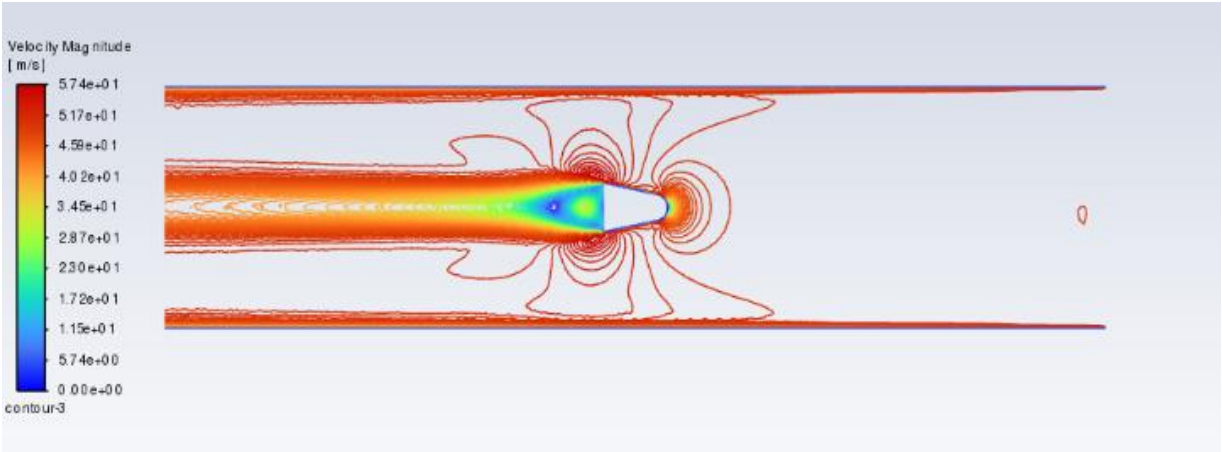

Finite

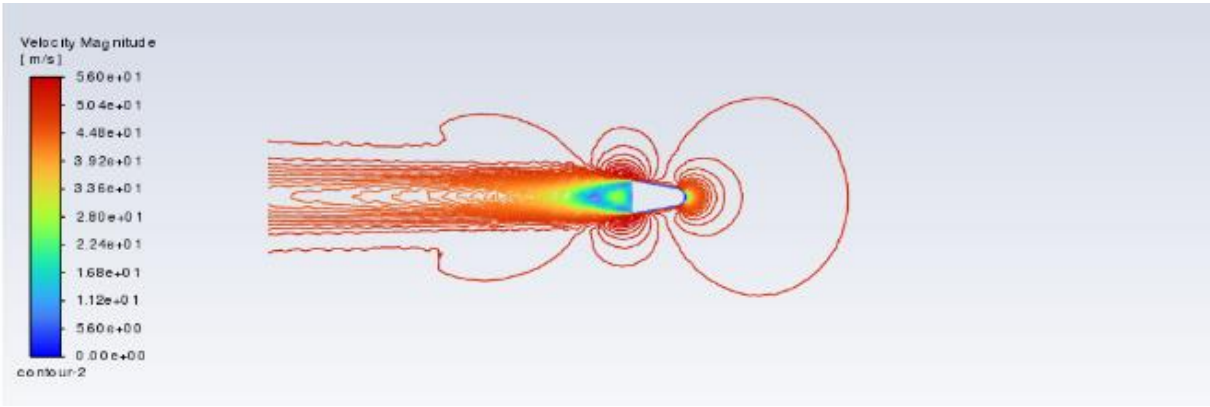

Infinite

Fig 15: Velocity Contours for cone 4 both finite and infinite domains for (a) Re = 84459, (b) Re = 168918, (c) Re = 337837, (d) Re = 675675

From figure 15, it is clear that for cone 4, the effect of tunnel interference is much more pronounced than in any other case. The velocity contour patterns of the confined and unconfined flows are significantly different than each other. The velocity gradients in the vicinity of the body are much larger for the confined flow than for the unconfined flow. Consequentially, the error in drag measurement is largest for cone 4, as has been clearly portrayed in figures 10 and 11.

3.3. Effect of supporting system interference on measurement of drag

In almost all experiments conducted in the wind tunnels, the model is attached with some kind of measuring instrument in order to record the forces that are acting on the body. However, the presence of this measuring instrument inadvertently affects the flow field around the model and results in inaccuracy of the force that it measures. To investigate these effects, the following analysis was performed.

Each of the cones was mounted on a measuring instrument, the dimensions of which were derived from a standard sting balance. The resulting body was placed inside the finite domain. The drag force on the body in this set up was computed and compared with those obtained from the body in the finite domain.

The results have been shown below.

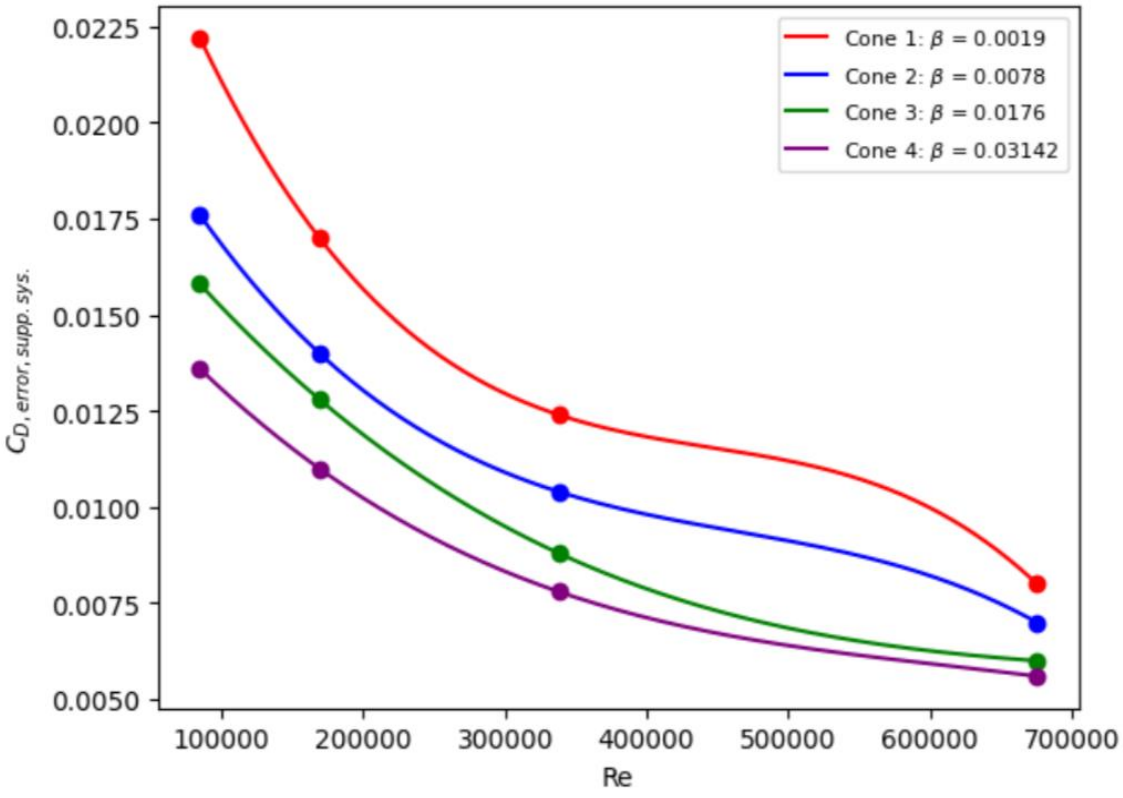

Fig 16: $C_{D,error,supp.sys.}$ vs Re at different β

Here, the term $C_{D,error,meas.sys}$ has been defined as

$$C_{D,error,supp.sys} = C_{D,supp.sys.} - C_{D,finite} \quad (9)$$

Here, $C_{D,supp.sys.}$ refers to the coefficient of drag on the model that has been computed when the model was mounted on the support system.

Figure 10 shows the difference between the absolute values of the coefficients of drag between the case with a supporting system and that without it. However, merely knowing their difference is not enough to show us the relative effect of the presence of supporting system. So, it might be beneficial to find the percentage change of drag experienced by the body due to the presence of the supporting system. This has been shown in figure 11, where

Also, Error due to supporting system % = $(C_{D,error,supp.sys} / C_{D,finite})$ X 100 (10)

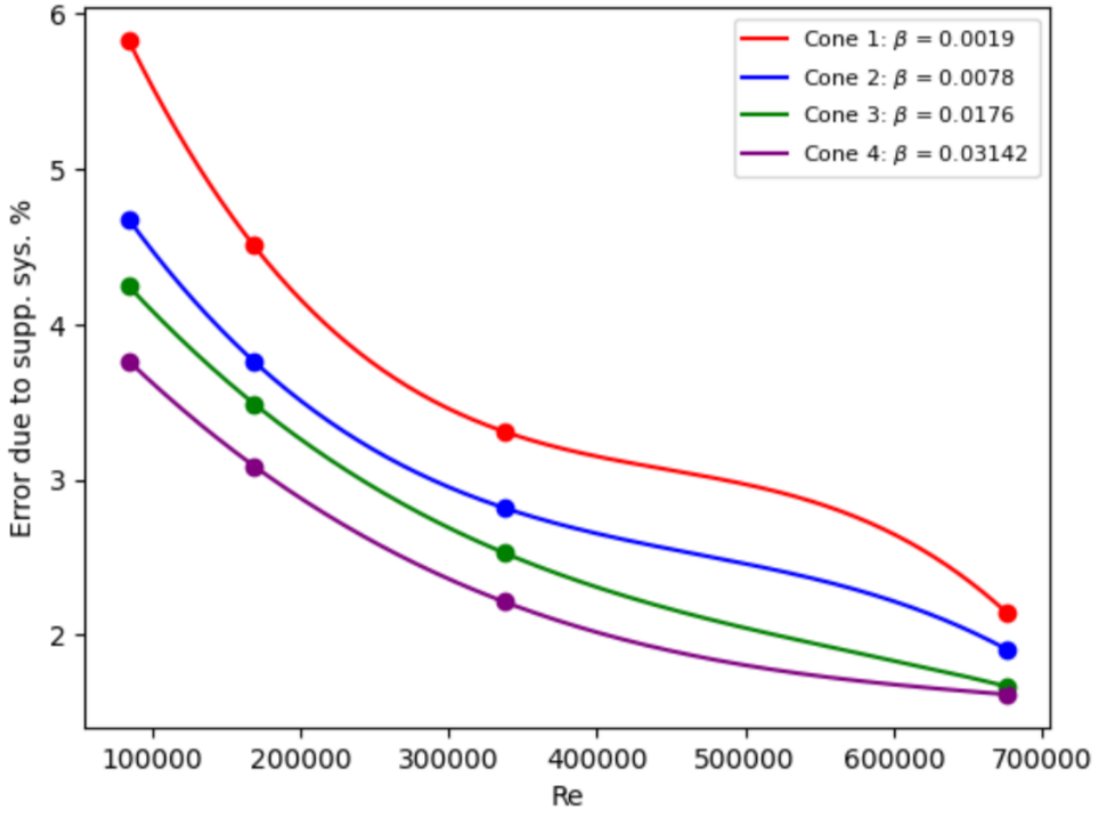

Fig 17: Percentage Error due to supporting system Vs Re for different blockage ratios

From figure 10, it can be seen that the value of $C_{D,error,supp.sys}$ is always positive, which indicates that the presence of the measurement system increases the drag on the model. The reason can be attributed to the fact that the measuring system increases the width of the wake and hence the drag increases.

From figures 10 and 11, it is clear that the effect of the presence of the measuring system in the flow field is more significant for cone 1 than for cone 4, i.e. this effect is more pronounced for flows in which the blockage ratio is lower. A possible explanation for this is that at low blockage ratios, the flow field around the body is quite similar to what it would have been in case of unconfined flow. So, the presence of measurement system significantly alters the flow field around the body. Since the body is placed closer to one wall than the other, the boundary layers formed on the wall closer to the body interacts with the wake and introduces an additional drag force on the body. This effect is less severe for flows with large blockage ratios.

The effect of the presence of the measurement system on the flow filed around the body has been shown in the figures below.

(a)

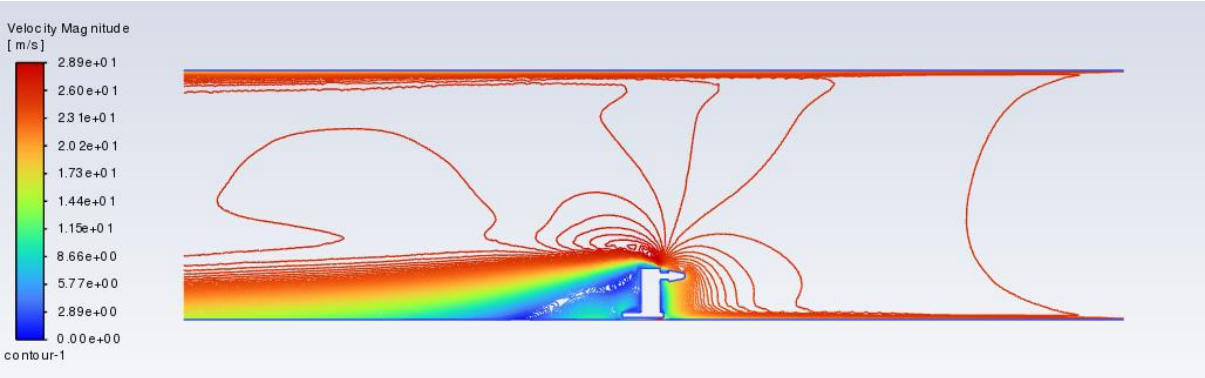

(b)

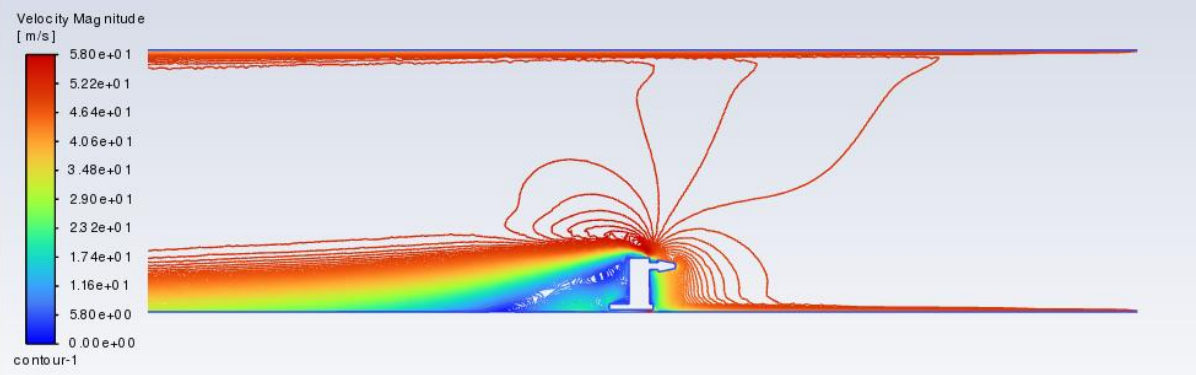

(c)

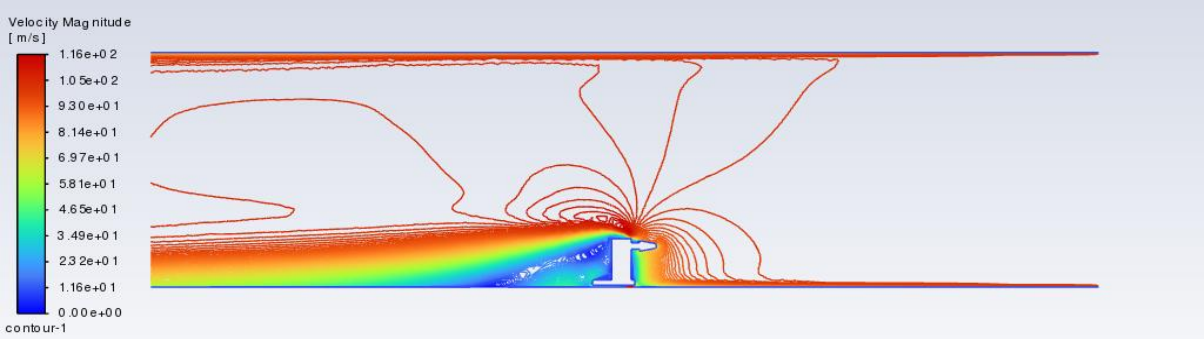

(d)

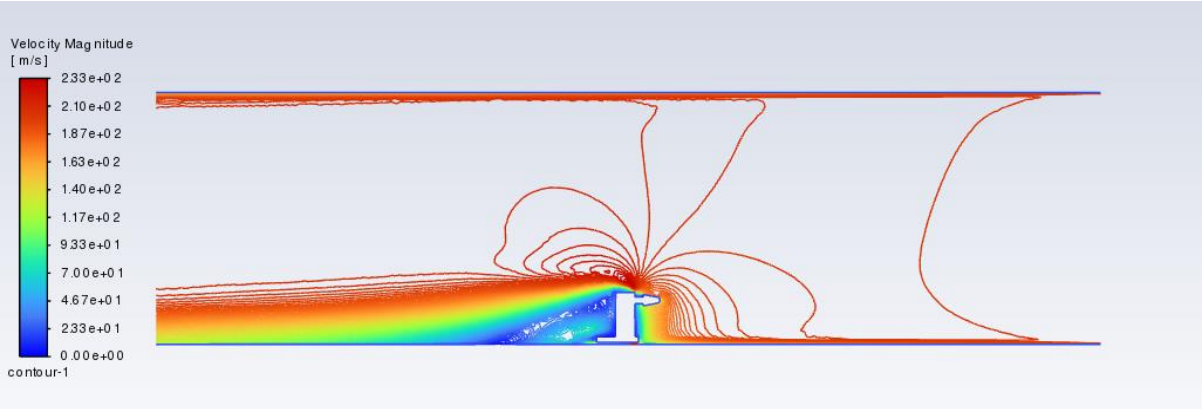

Fig 18: Velocity contours for Cone 1 with supporting system for (a) Re = 84459, (b) Re = 168918, (c) Re = 337837, (d) Re = 675675

A careful observation of figures 6 and 12 indicates that the patterns of the velocity contours for cone 1 with and without the measurement system show drastic changes. Firstly, the velocity contours have become asymmetric in figure 12, which indicates that the flow field itself has become asymmetric. This is mainly because in figure 12, the whole setup has been placed nearer to one wall. So, the cone is closer to one wall than the other which gives rise to the asymmetry. Also,

as mentioned before, the wake is much wider in figure 12 than in figure 6, which is a direct consequence of the presence of the measurement system.

(a)

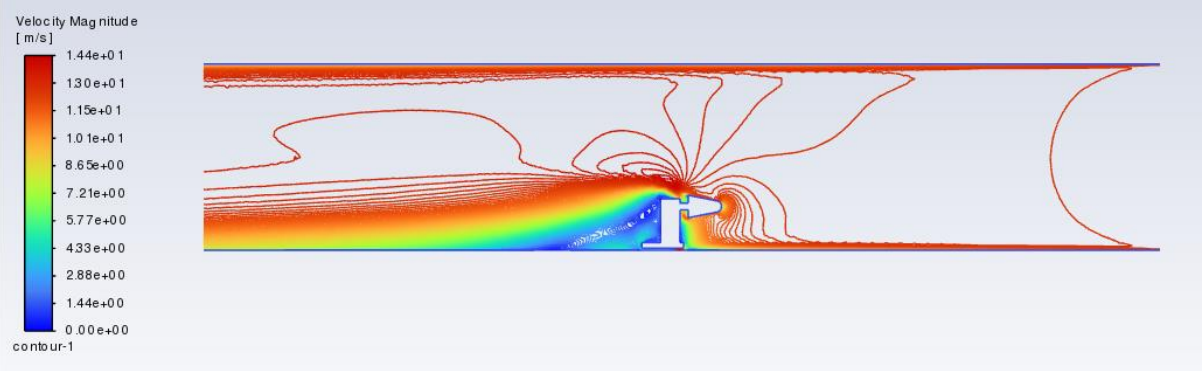

(b)

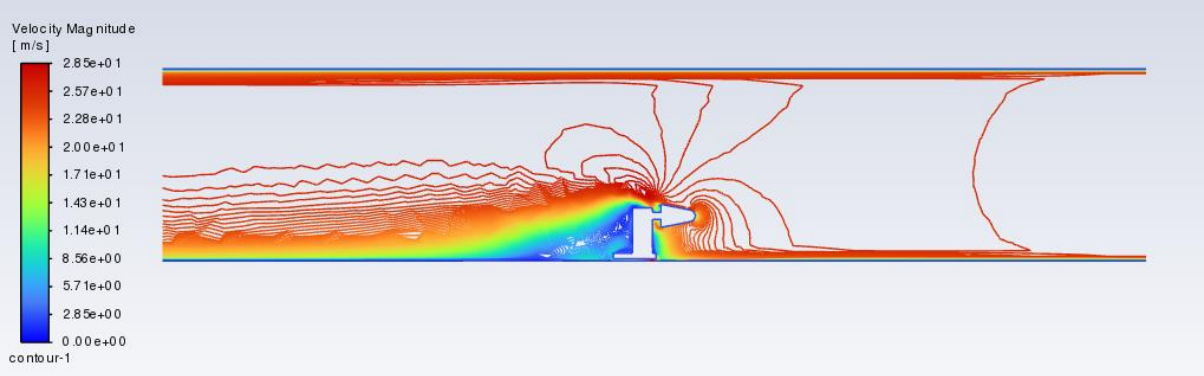

(c)

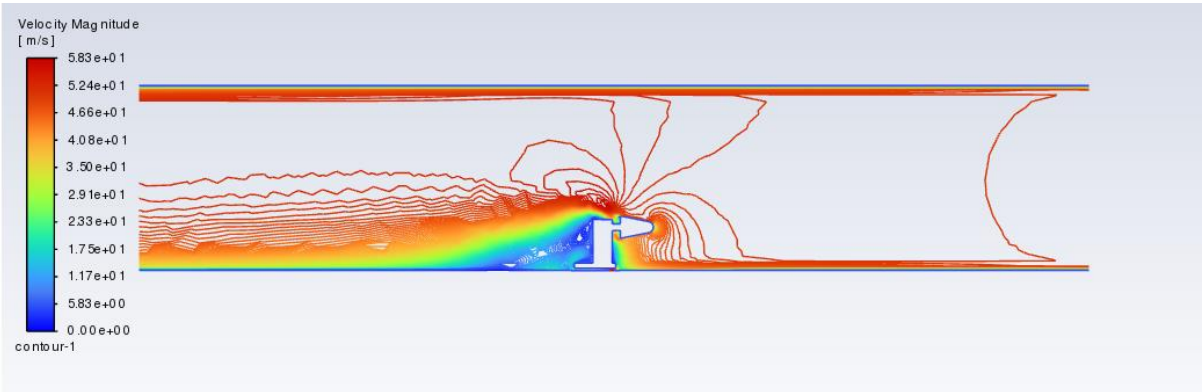

(d)

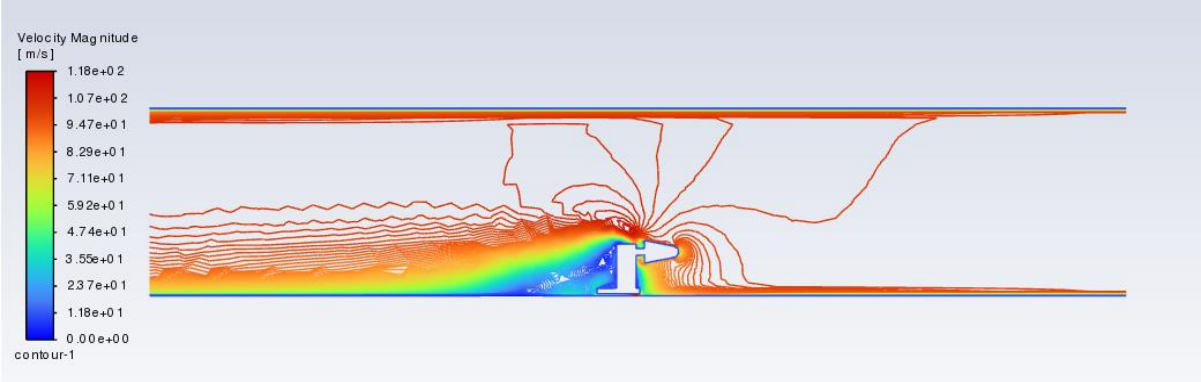

Fig 19: Velocity contours for Cone 2 with supporting system for (a) Re = 84459, (b) Re = 168918, (c) Re = 337837, (d) Re = 675675

From figures 7 and 13, we can see that the velocity profiles are quite different from each other. The width of the wake in figure 13 is greater than that in figure 7. Also, the velocity contour pattern is asymmetric in figure 13. Consequently, the drag coefficient on cone 2 with measurement system is more than that without the measurement system.

(a)

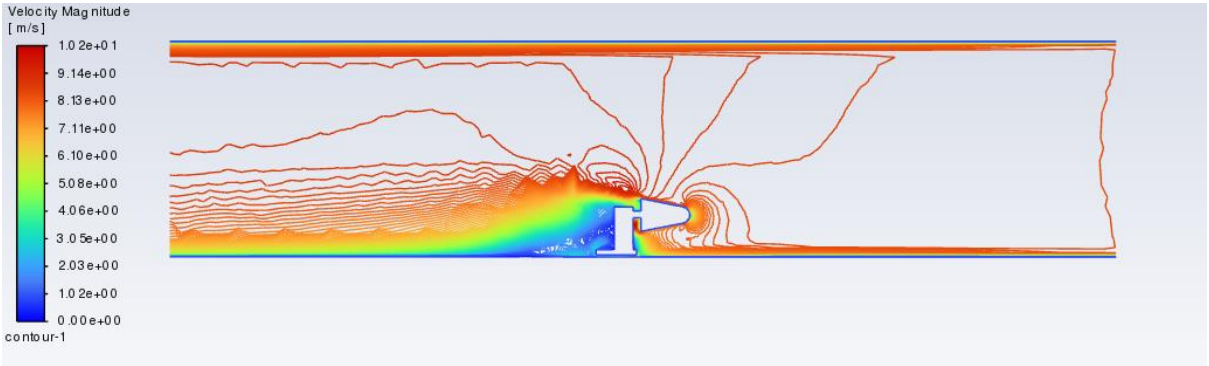

(b)

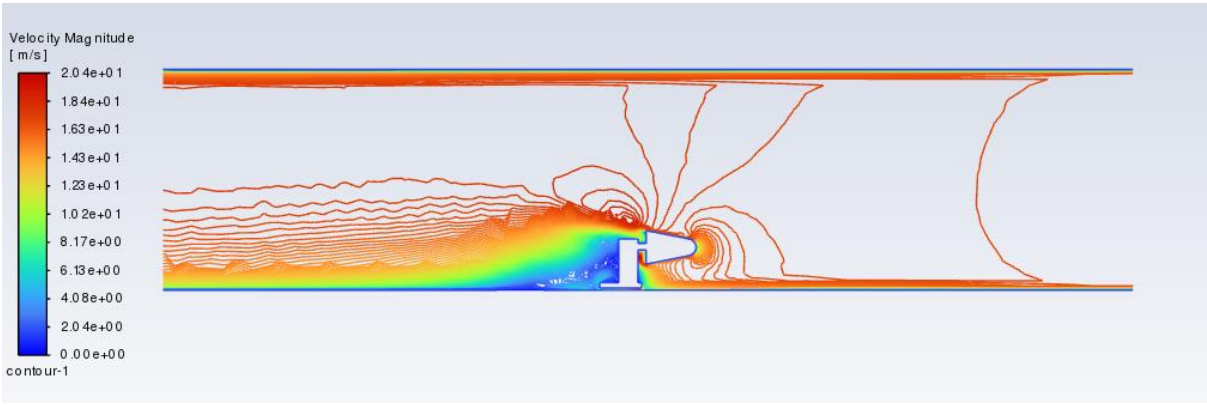

(c)

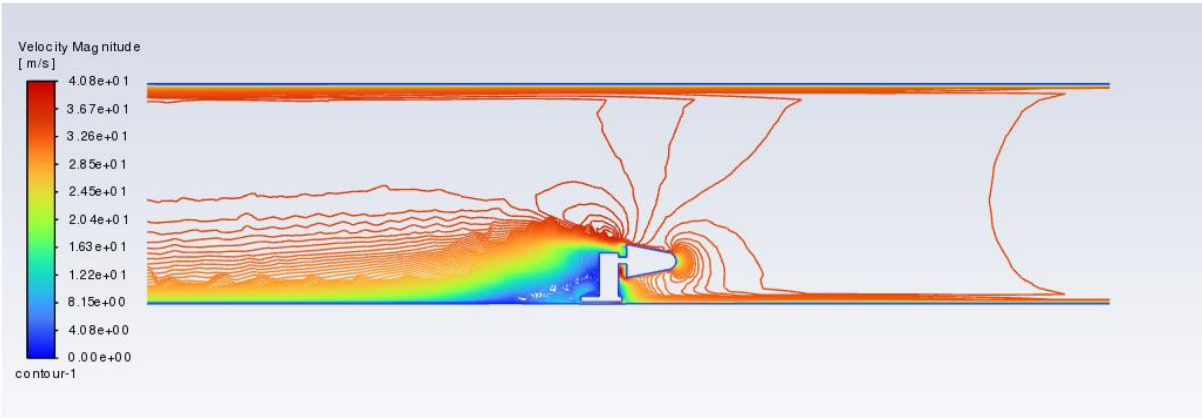

(d)

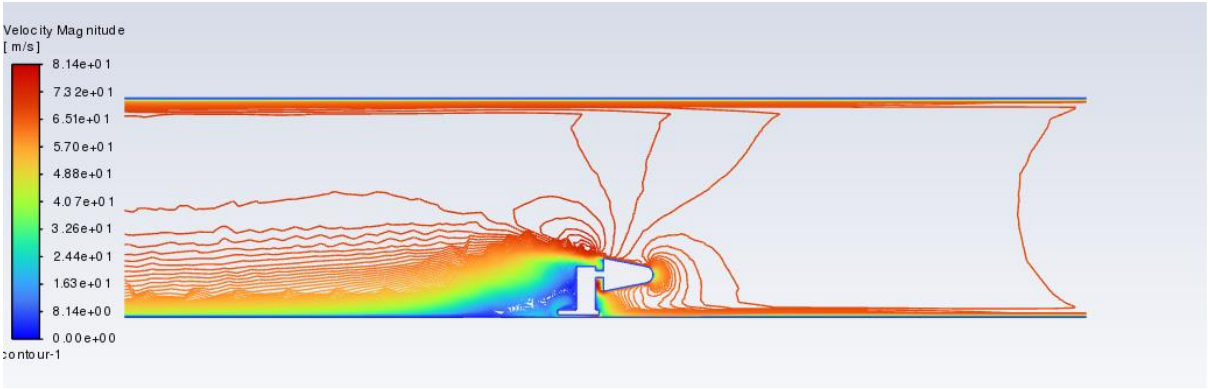

Fig 20: Velocity contours for Cone 3 with supporting system for (a) Re = 84459, (b) Re = 168918, (c) Re = 337837, (d) Re = 675675

From figures 8 and 14, we can see that again the flow fields are significantly different from each other. Similar to what is stated above, the wake is wider for the case with the measurement system and the flow field is asymmetric. The drag on the body is more with the measurement system than without it.

(a)

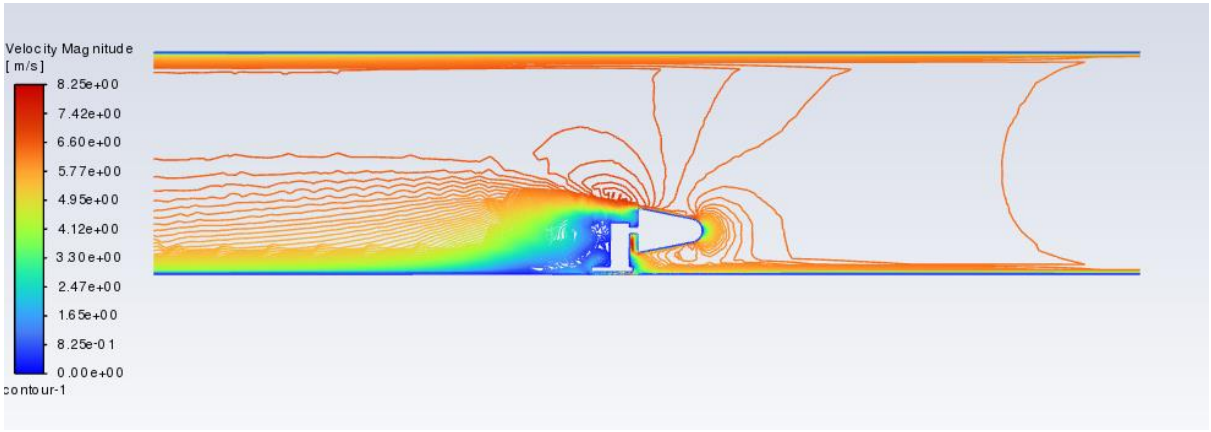
Velocity Magnitude
[m/s]
8.25e+00
7.42e+00
6.60e+00
5.77e+00
4.95e+00
4.12e+00
3.30e+00
2.47e+00
1.65e+00
8.25e-01
0.00e+00
contour-1

(b)

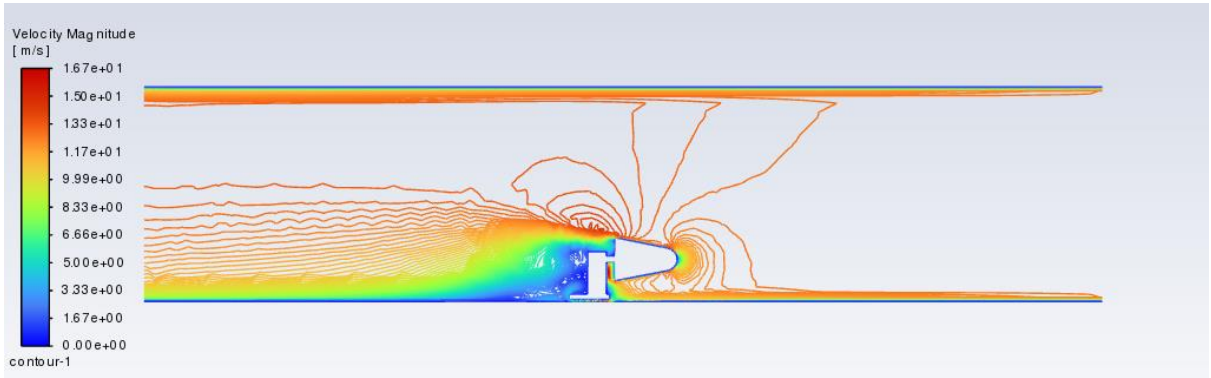
Velocity Magnitude
[m/s]
1.67e+01
1.50e+01
1.33e+01
1.17e+01
9.99e+00
8.33e+00
6.66e+00
5.00e+00
3.33e+00
1.67e+00
0.00e+00
contour-1

(c)

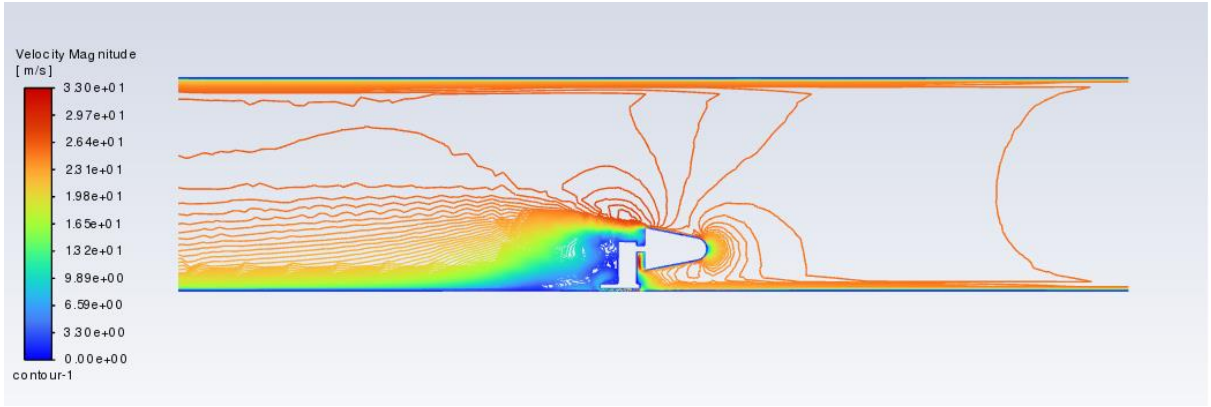
Velocity Magnitude
[m/s]
3.30e+01
2.97e+01
2.64e+01
2.31e+01
1.98e+01
1.65e+01
1.32e+01
9.89e+00
6.59e+00
3.30e+00
0.00e+00
contour-1

(d)

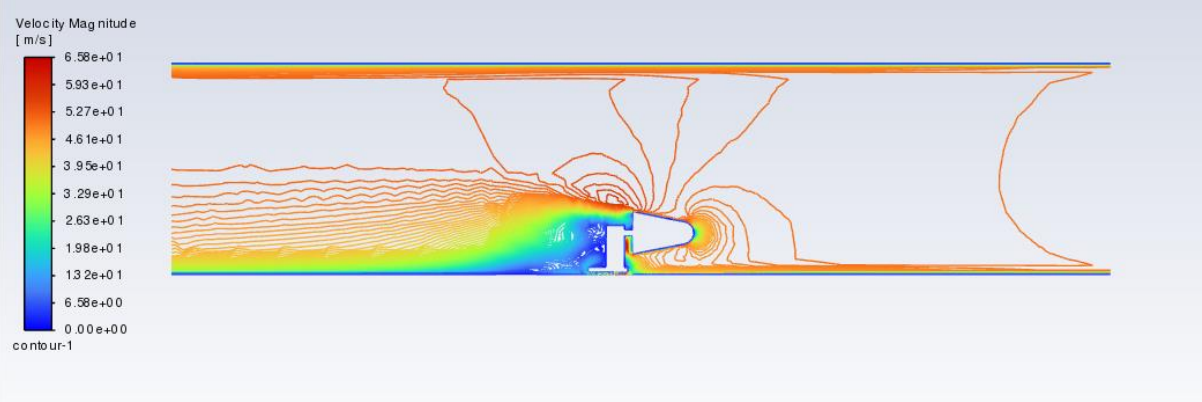

Fig 21: Velocity contours for Cone 4 with measurement system for (a) Re = 84459, (b) Re = 168918, (c) Re = 337837, (d) Re = 675675

From figures 9 and 15, we can see that the flow fields are significantly different from each other. Similar to the discussion above, the width of the wake is greater for the case with the measurement system and the flow field is asymmetric. The drag on the body is more with the measurement system than without it.

The discussion above shows the effect that the presence of supporting system has on the flow field around the body in a finite domain. However, the finite domain itself fails to simulate the actual flow field that would exist in an unconfined flow. The actual flow field in an unconfined flow around is well simulated by the infinite domain. Hence, a comparison between the drag computed in the infinite domain and that computed in the presence of a support system needs to be performed to highlight the actual deviation of the results from the unconfined flow. This has been done below, in figure.

3.4. Error in drag measurement due to cumulative effect of tunnel and supporting system interference

To compare the error in computing the drag due to the effect of both tunnel interference and support system interference, the difference between the drag coefficients for the cones with supporting systems (finite domain) and without

supporting system (infinite domain) have been calculated. Then, the total drag percentage has been calculated as

total error percentage in drag = $(C_{D,supp.sys.} - C_{D,infinite}) / C_{D,infinite}$ X 100 (11)

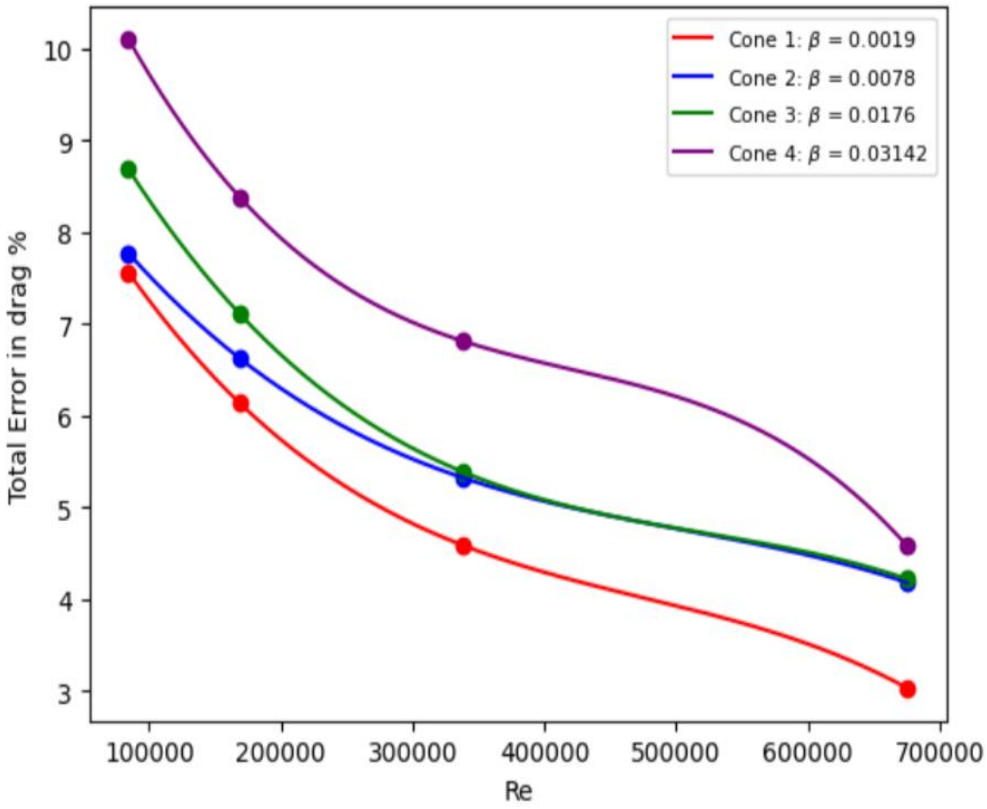

Fig 22: Total error percentage in drag vs Re for different blockage ratios

From the figure 22, it can be seen that the total error percentage in drag measurement increases with increase in blockage ratio for a given Reynolds' number. Intuitively, this result makes sense, because a higher blockage ratio means more tunnel interference. Moreover, for a given blockage ratio, the total error percentage decreases with increase in Reynolds' number. This is because, again, although the absolute value of the error increases, the drag coefficient in infinite domain increases much faster and hence the error percentage decreases.

Chapter 4:

Conclusion and Future Scope

4.1. Conclusion

In the above analysis, the effect of tunnel interference and supporting system interference on drag coefficient has been portrayed. It is found that the tunnel interference increases with increase in blockage ratio, while decreasing with increasing Reynolds' number. However, the supporting system interference seems to decrease with increase in both blockage ratio and Reynolds' number. Since both types of interferences are present while measuring drag in wind tunnel experiments, it is imperative to consider the total error in drag measurement due to both these interferences. It has been found in this study that the total error in drag measurement increases with increase in blockage ratio and decreases with increase in Reynolds' number. It therefore follows that, the wind tunnel experiments conducted at high Reynolds' numbers and low blockage ratios are expected to involve the least error in drag measurement.

4.2. Future Scope

The above analysis has been performed purely by numerical simulation and hence the experimental validation of these results has to be performed. Moreover, since this thesis encompasses only conical bluff bodies, some other shapes for the bluff bodies should be considered for similar analysis in the future.

References

1. Maskell E.C., “A theory of blockage effect on bluff bodies and stalled wings in a closed wind tunnel”, Aeronautical Research Council: Reports and Memoranda 3400(1963)
2. Modi V.J., El-Sherbiny S.E., “A free-streamline model for bluff bodies in confined flow”, J. of Fluids Eng. 97 (1977)
3. Petty D.G., “The effect of turbulence intensity and scale on the flow past square prisms”, J. of Industrial Aerodynamics 4 (1979)
4. Mondal R.N., Alam M.M., “Blockage effect on wakes of various bluff bodies: A review of confined flows”, J. of Ocean Engineering 286 (2023)
5. Stanlaker J.F., Hussey R.G., “Wall effect in cylinder drag at low Reynolds’ number”, Phys. Fluids 22(1979)
6. Chakraborty J., Verma N., Chhabra R.P., “Wall Effects in Flow Past a Circular Cylinder in a Plane Channel: A numerical study”, J. of Chemical Engineering and Processing 43(2004)
7. Kumar P., Singh S.K., “Flow past a bluff body subjected to lower subcritical Reynolds’ number”, J. of Ocean Engineering and Science 5(2020)
8. Kannaris N., Grigoriadis D., Kassinos S., “Three dimensional flow around a circular cylinder confined in a plane channel”, J. of Phys. Fluids. 23(2011)
9. Aljubaili D., Chan L., Lu W., Ooi A., “Numerical investigation of the wake behind a confined flat plate”, Int. J. of Heat Fluid Flow 94(2022)
10. Nguyen Q.D., Lei C. , “Hydrodynamic characteristics of a confined circular cylinder in cross-flows”, J. of Ocean Eng. 221(2021)
11. Mishra S.K., Kumar D., Sourav K., Yadav P.K., Sen S., “Highly confined flow past a stationary square cylinder”, Advances in Fluid and Thermal Engineering. Lecture Notes in Mechanical Engineering, Springer, Singapore (2019)

12. Sohankar A., Norberg C., Davidson L., “Simulation of three-dimensional flow around a square cylinder at moderate Reynolds’ number”, Phys. Fluids 11(1999)
13. Mukhopadhyay A., Biswas G., Sundararajan T., “Numerical Investigation of confined wakes behind a square cylinder in a channel”, Int. J. of Num. Methods Fluid. 14(1992)
14. Takeuchi M., Okamoto T., “Effect of side-walls of wind tunnel on turbulent wake behind two-dimensional bluff body”, In: Proceedings of the Fourth Symposium on Turbulent Shear Flows, Karlsruhe, Germany, September 12-14, 1983, 5.25-5.30 (1983)
15. Uhlherr P.H.T., Chhabra R.P., “Wall effect for the fall of spheres on cylindrical tubes at high Reynolds’ numbers”, J. of Chem. Eng. 73(1995)
16. Chhabra R.P. , Agarwal S., Chaudhary K.,, “A note on wall effect on the terminal falling velocity of a sphere in a quiescent Newtonian media in cylindrical tubes”, J. Powder Tech. 129(2003)
17. Krishnan S. , Kaman A., “Effect of blockage ratio on drag and heat transfer from centrally located sphere in pipe flow”, J. Eng. Appl. Comput. Fluid Mechanics 4(3) (2010)
18. Kuwaguti M., Jain P., “Numerical study of a viscous fluid flow past a circular cylinder”, J. of Phys. Soc. Jpn. 21(1966)
19. Hamielec A.E., Raal J.D. , “Numerical study of viscous flows around circular cylinders”,J. of Phys. Fluid 12(1969)
20. Dennis S.C.R., Chang G.Z., “Numerical solutions for steady flow past a circular cylinder at Reynolds’ number up to 100”, J. of Fluid Mech. 42(1970)
21. Sucker D., Brauer H., “Fluiddynamik bei quer angestromten Zylindern”,Warme- und Stoffubertragung 8 (1975)

22. (a) Fornberg B. , “A numerical study of steady viscous flow past a circular cylinder”, J. of Fluid Mech. 98 (1980)
(b) Fornberg B., “Steady viscous flow past a circular cylinder up to Reynolds’ number 600”, J. of Comp. Phys. 61 (1985)
23. Rajani B.N., Kandasamy A., Majumdar S., “Numerical simulation of laminar flow past a circular cylinder”, J. of Appl. Math. Model 33 (2009)
24. Dhiman A., Shyam R., “Unsteady heat transfer from an equilateral triangular cylinder in the unconfined flow regime”, ISRN Mech. Eng. 2011(2011)
25. Chatterjee D., Mondal B., “Forced convection heat transfer from an equilateral triangular cylinder at low Reynolds numbers”, Int. J. of Heat. Mass. Transf. 48(2012)
26. Pawar A.P., Sarkar S., Saha S.K., “Forced convective flow and heat transfer past an unconfined blunt headed cylinder at different angles of incidence”, J. of Appl. Math. Model. 82 (2020)
27. List R. , Schemenauer R.S., “Free fall behaviour of planar snow crystals, conical graupel and small hail”, J. Atmos. Sci. 28(1971)
28. Sharma M.K., Chhabra R.P., “An experimental study of free fall of cones in Newtonian and non-Newtonian media: drag coefficient and wall effects” J. of Chem. Eng. Process. 30(1991)
29. Samantaray S.K., Mohapatra S.S., Munshi B., “A numerical study of wall effects for Newtonian fluid flow over a cone” Int. J. of Eng. Sc. Tech. 20(2017)
30. Ocokoljic G., Rasuo B., Kozic M., “Supporting system interference on aerodynamic characteristics of an aircraft model in a low speed wind tunnel”, J. of Aero. Sci. Tech. 64(2017)
31. Cartieri A., Viscat P., Mouton S., ”Using CFD to calculate support interference effect in wind tunnel tests”, 47th Symposium of Appl. Aerodyn. (Mar. 2012), Paris, France

32. Mouton S., “Numerical Investigation of model support interference in a transonic wind tunnel”, 44th Symposium of Appl. Aerodyn. (Mar. 2009), Nantes, France
33. Menter F.R., Lechner R., Matyushenko A., “Best Practice: Generalized k-ω (GEKO) Two-Equation Turbulence Modeling in Ansys CFD”, ANSYS guidebook (2021)